Supplementary Information

克级自下向上闪蒸石墨烯合成

Gram-scale bottom-up flash graphene synthesis

Duy X. Luong,[1,2] Ksenia V. Bets,[3] Wala Ali Algozeeb,[2] Michael G. Stanford,[2] Carter Kittrell,[2] Weiyin Chen,[2] Rodrigo V. Salvatierra,[2] Muqing Ren,[2] Emily A. McHugh,[2] Paul A. Advincula,[2] Zhe Wang,[2] Mahesh Bhatt,[4] Hua Guo,[3] Vladimir Mancevski,[2] Rouzbeh Shahsavari,[4,5*] Boris I. Yakobson,[2,3,6*] and James M. Tour[2,3,6*]

[1]Applied Physics Program, [2]Department of Chemistry, [3]Department of Materials Science and NanoEngineering,

Rice University, 6100 Main Street, Houston, Texas 77005, USA

[4]C-Crete Technologies, 13000 Murphy Rd, Unit 102, Stafford, TX 77477, USA

[5]Department of Civil and Environmental Engineering, [6]Smalley-Curl Institute and the NanoCarbon Center,

Rice University, 6100 Main Street, Houston, Texas 77005, USA

设备
Equipment. Page 4

补充图1. FJH系统。
Supplementary Fig. 1. FJH system. Page 4

FJH组件列表
FJH Components list. Page 5

警告：存在触电甚至触电的风险，因此应实施这些功能。
CAUTION: There is a risk of electrical shock or even electrocution, so these features should be implemented. Page 6

高碳材料转化为FG的估计能量。
Estimated energy for conversion of high carbon materials into FG. Page 8

拉曼分析和涡轮层状石墨烯的讨论。
Discussion of Raman Analyses and Turbostratic Graphene. Page 8

石墨烯被定义为二维材料。
Graphene is defined as a 2-D material. Page 8

拉曼光谱作为二维特征的确定标准。
Raman as a definitive standard for 2-D character. Page 10

涡轮层石墨与涡轮层石墨烯。
Turbostratic graphite vs. turbostratic graphene. Page 10

层数不定义二维特征。
Number of layers does not define 2-D character. Page 11

使用TS1和TS2作为正面指标。
Using TS_1 and TS_2 as positive indicators. Page 12

消失的M带。
The silent M band. Page 12

补充图2。CB-FG拉曼光谱中的涡轮层峰。
Supplementary Fig. 2. Turbostratic peaks in the Raman spectrum of CB-FG. Page 13

补充图3。CB-FG拉曼光谱中的2D峰。
Supplementary Fig. 3. 2D peak in the Raman spectrum of CB-FG. Page 14

CB-FG的拉曼光谱与已报道的涡轮层状石墨烯的拉曼光谱的比较。
Comparison of the Raman spectrum of CB-FG to those in reported turbostratic graphene. Page 15

补充表1: 2D、TS1和TS2峰值与之前研究的比较。
Supplementary Table 1: Comparison of 2D, TS_1 and TS_2 peak with previous studies. Page 15

非常小的D带。
The very small D-band. Page 16

补充图4。CB-FG的BET表面积分析。
Supplementary Fig. 4. BET surface area analysis of CB-FG. Page 16

补充表2。各种材料的FJH参数。
Supplementary Table 2. FJH parameters for various materials. Page 17

闪蒸石墨烯形态。
Flash Graphene Morphology. Page 18

补充表3。表报告了从每个碳源形成闪蒸石墨烯时石墨烯多面体或石墨烯片的存在。
Supplementary Table 3. Table reporting the presence of graphene polyhedra or graphene sheets when forming flash graphene from each carbon source. Page 21

补充图5。CB-FG和CPC-FG的尺寸分布。
Supplementary Fig. 5. Size distribution of CB-FG and CPC-FG. Page 22

补充图6。炭黑衍生FG的AFM表征。
Supplementary Fig. 6. AFM characterization of carbon black-derived FG. Page 23

补充图7。无烟煤和咖啡衍生FG的粒度分布。
Supplementary Fig. 7. Size distribution of anthracite- and coffee-derived FG. Page 24

补充图8。单层石墨烯的TEM图像。
Supplementary Fig. 8. TEM images of single layer of graphene. Page 25

补充图9。无烟煤衍生FG的SAED。
Supplementary Fig. 9. SAED of anthracite-derived FG. Page 26

补充图10。咖啡衍生FG的SAED。
Supplementary Fig. 10. SAED of coffee-derived FG. Page 27

补充图11。来自其他碳源的FG的代表性拉曼光谱。
Supplementary Fig. 11. Representative Raman spectra of FG derived from other carbon sources. Page 28

补充表4。补充图11的前体源。第29页
Supplementary Table 4. Precursor sources for Supplementary Fig. 11. Page 29

补充图12。超快温度测量。
Supplementary Fig. 12. Ultrafast temperature measurement. Page 30

补充图13. FJH工艺前后煅烧石油焦、预处理(见正文)咖啡渣和炭黑的XPS。
Supplementary Fig. 13. XPS of calcined petroleum coke, pre-treated (see main text) coffee grounds and carbon black before and after the FJH process. Page 32

补充图14。CB-FG和CPC-FG的C 1s光谱的高分辨率XPS。
Supplementary Fig. 14. High resolution XPS of the C 1s spectrum from CB-FG and CPC-FG. Page 33

补充图15. FJH前后TGA。
Supplementary Fig. 15. TGA before and after FJH. Page 34

补充图16。FG过程自动化的可能反应器。
Supplementary Fig. 16. Possible reactors for automation of the FG process. Page 35

补充图17。FG在水/Pluronic中的分散。
Supplementary Fig. 17. FG dispersion in water/Pluronic. Page 37

补充图18。CB-FG/水泥复合材料的力学性能。
Supplementary Fig. 18. Mechanical properties of the CB-FG/cement composites. Page 38

补充图19。水泥和CB-FG复合材料的SEM图像。
Supplementary Fig. 19. SEM images of cement and CB-FG composite. Page 39

补充图20。PDMS、CB-FG/PDMS复合材料和CB/PDMS复合材料。
Supplementary Fig. 20. Compressive strength of PDMS, CB-FG/PDMS composite and CB/PDMS composite. Page 40

补充图21。FG在锂离子电容器和锂离子电池中。
Supplementary Fig. 21. **FG in a Li-ion capacitor and a Li-ion battery. Page 41**

电化学测试方法。
Electrochemical Test Protocols. Page 42

References. Page 43

设备
Equipment

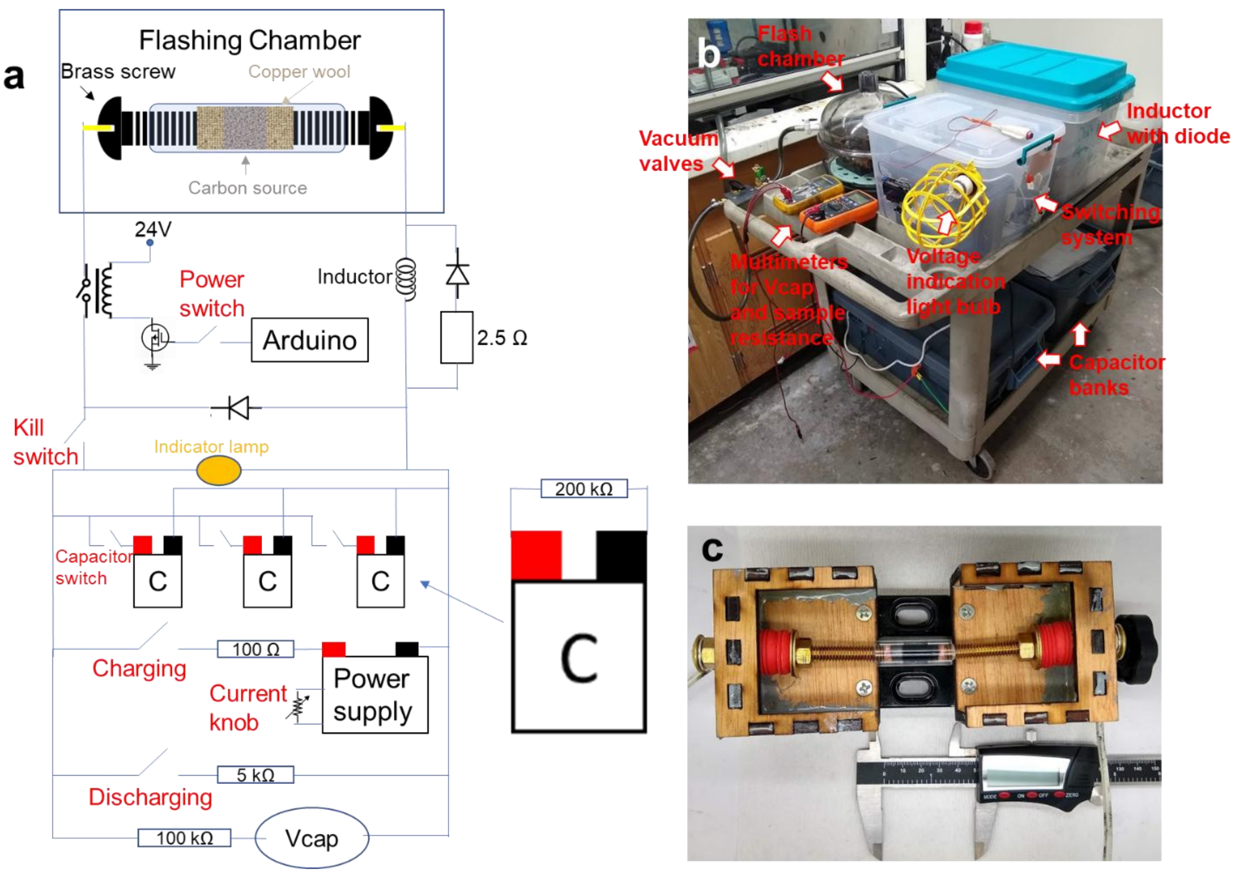

补充图1. FJH系统。 FJH系统的电气示意图。 安装在塑料车上的系统照片。 样品架由小型商用台钳(Amazon)和激光切割的木制零件制成。 松散配合(允许气体在闪蒸期间逸出)的黄铜螺钉充当两个电极，与接触所需碳源的铜丝塞(或石墨盘)接触。 红色橡胶塞可逐渐压缩样品,
Supplementary Fig. 1. FJH system. **a**. Electrical schematic of the FJH system. **b**. Photograph of the system set up on a plastic cart. c. The sample holder that is made from a small commercial vise (Amazon) and laser cut wooden parts. The loosely fitting (to permit gas escape during flashing) brass screws act as two electrodes that contact the copper wool plugs (or graphite disks) that touch the desired carbon source. Red rubber stoppers provide gradual compressing of the

而虎钳被压缩以增加样品的电导率。 卡钳宽度为5厘米。
sample while the vice is compressed to increase the conductivity of the sample. Caliper width is 5 cm.

FJH部件清单：
FJH Components list:

-电容器：10x450 V，6 mF铝电解电容器(Mouser#80- 该电容器组用于FG合成，批量为0.5 g
- Capacitor: 10x of 450 V, 6 mF aluminum electrolytic capacitors (Mouser #80-PEH200YX460BQU2). This capacitor bank is for FG synthesis with batch sizes ≤0.5 g

-10 x 400 V，18 mF铝电解电容器(Mouser#80-ALS70A183QS400)。
- 10x of 400 V, 18 mF aluminum electrolytic capacitors (Mouser # 80-ALS70A183QS400).

  该附加电容器组用于批量大于0.5 g且小于等于1.0 g的FG合成
  This additional capacitor bank is for FG synthesis with batch sizes >0.5 g and up to 1.0 g

-机械继电器：900 V，500 A(TE连接性LEV200A5ANA)
- Mechanical relay: 900 V, 500 A (TE Connectivity LEV200A5ANA)

-电源：LED电源299.6W 214-428V 700mA(Mouser #709 -电流旋钮为10 k电位计
- Power supply: LED Power Supplies 299.6W 214-428V 700mA (Mouser # 709-HLG320H-C700B). Current knob is a 10 kΩ potentiometer

-Vcap由万用表福禄克189测量
- Vcap is measured by a multimeter Fluke 189

-放电和充电开关断路器：400 V，6A(ABB S 282 K 6A)
- Discharging and charging switch breaker: 400 V, 6A (ABB S 282 K 6A)

-电容开关断路器：277 V，10 A(ABB S201P-C10)
- Capacitor switch breaker: 277 V, 10 A (ABB S201P-C10)

-压井开关断路器：440 V，63 A(AAB S283 UC Z 63A)
- Kill switch breaker: 440 V, 63 A (AAB S283 UC Z 63A)

-控制器：Arduino Uno，带LCD显示屏
- Controller: Arduino Uno with LCD display

-电感器：24 mH(Mouser#553-C-80U)
- Inductor: 24 mH (Mouser #553-C-80U)

-二极管：1200 V，560 A(Mouser#747-MDO500-12N1)
- Diode: 1200 V, 560 A (Mouser #747-MDO500-12N1)

警告：存在触电甚至触电的风险，因此应实施这些功能。 该列表并不全面，但说明了最小化风险所需的规则。
CAUTION: There is a risk of electrical shock or even electrocution, so these features should be implemented. This list is not intended to be comprehensive but demonstrative of the protocols needed to minimize risk.

1、封闭或小心绝缘所有接线。
1. Enclose or carefully insulate all wire connections.

2、所有连接、电线和部件必须适合高电压和高电流。
2. All connections, wires and components must be suitable for the high voltages and currents.

3、请注意，部件故障可能会导致高压出现在意外的地方，例如开关晶体管上的散热器。
3. Be aware that component failure could cause high voltage to appear in unexpected places, such as heat sinks on the switching transistors.

4、控制线应具有额定高压的光隔离器。
4. Control wires should have opto-isolators rated for high voltage.

5、提供可见的充电指示灯。230 V透明玻璃白炽灯泡是一个不错的选择，因为灯丝上的辉光还提供了电容器组上电荷量的近似指示器。亮光=危险！
5. Provide a visible charge indicator. A 230 V clear glass incandescent light bulb is a good choice as the glow on the filament also provides an approximate indicator of the amount of charge on the capacitor bank. Bright light = danger!

6、不要将手动开关与金属开关一起使用。如果产生电弧，金属开关可能带电。
6. Do not use toggle switches with metal toggles. If an arc develops, the metal toggle could become charged.

7、单手定则。在系统上工作时，只使用一只手，另一只手不要接触任何接地表面。
7. One hand rule. Use only one hand when working on the system, with the other hand not touching any grounded surface.

8、在每个电容器上安装100000欧姆范围内的放电电阻器，以便在约1小时内始终泄放电荷。
8. Install bleed resistors in the range of 100,000 ohms on each capacitor so that charge will always bleed off in ~1 h.

9、提供一个连接到几百欧姆功率电阻器的机械放电断路器开关，以快速释放电容器电荷。
9. Provide a mechanical discharge circuit breaker switch connected to a power resistor of a few hundred ohms to rapidly bleed off the capacitor charge.

10、提供一个“切断”断路器开关，以断开样品架与电容器组的连接。
10. Provide a "kill" circuit breaker switch to disconnect the sample holder from the capacitor bank.

11、提供交流断路器开关。
11. Provide an AC disconnect circuit breaker switch.

12、在设备上张贴高压警告标志。
12. Post high voltage warning signs on the apparatus.

13、将断路器用作开关。断路器具有内置消弧功能，可中断1000安培或更大电流。传统开关没有如此高的消弧水平，可能会因高电流脉冲而烧坏或焊接闭合。
13. Use of circuit breakers as switches. Circuit breakers have built-in arc suppression that can interrupt 1000 amps or more. Conventional switches do not have such a high level of arc suppression and can burn out or weld closed due to the high current pulses.

14、使用额定直流电压的断路器。 大多数交流断路器的直流额定值为电压的1/2或更低，因为直流电弧更难抑制。 为直流太阳能发电系统设计的断路器是一个不错的选择。

14. Use circuit breakers rated for DC voltage. Most AC circuit breakers have a DC rating 1/2 the voltage or less, since DC arcs are much more difficult to suppress. Circuit breakers designed for DC solar power systems are a good choice.

15、选择断路器时，根据0.1 s的典型时间曲线进行选择，而不是稳态额定电流。 与额定电流相比，K型直流断路器在0.1 s时的跳闸电流将增加约10倍，Z型断路器在0.1 s时的跳闸电流将增加约4倍。 大多数断路器中设计的这种“ 延迟跳闸 ”将允许比断路器稳态额定值高得多的脉冲电流。

15. When choosing circuit breakers, choose by the time curves typical for 0.1 s, rather than the steady state current rating. K-type DC circuit breakers will have ~10x higher trip current at 0.1 s compared to their rated current, and Z-type breakers will have ~4x higher trip current at 0.1 s. This "delayed trip" designed into most circuit breakers will allow much higher pulse currents than the steady state rating of the breaker.

16、在放电电路中加入少量电感，以将上升时间限制在毫秒或更高。 极快的放电会损坏部件，并对其他实验室设备造成射频干扰。

16. Include a small amount of inductance in the discharge circuit to limit the rise time to a millisecond or more. Extremely fast discharges can damage components and cause RF interference with other lab apparatus.

17、请记住，系统可以在毫秒内放电数千焦耳，这可能导致继电器甚至电容器等部件爆炸。 这些部件应封闭起来，以防止高压和可能的飞屑。

17. Keep in mind that the system can discharge many thousands of Joules in milliseconds, which can cause components such as relays or even capacitors to explode. These components should be enclosed to protect against both high voltage and possible flying debris.

18、始终将带有高压测试引线的电压表放在手边。 在电容器组上工作时，务必检查每个电容器组上的电压。 断线或连接松动可能使电容器处于充电状态。

18. Keep a voltmeter with high voltage test leads handy at all times. When working on the capacitor bank, always check the voltage on each. A broken wire or loose connection could leave the capacitor in a charged state.

19、使用仪器时，戴上厚厚的橡胶手套，以防触电。

19. Wear thick rubber gloves when using the apparatus to protect from electrocution.

所有用户均应由经验丰富的电气技术人员进行适当培训。

20. All users should be properly trained by an experienced electrical technician.

使用这些设计和安全参数，实验室规模的设备很可能会商业化。

Commercialization of laboratory-scale equipment will likely follow using these design and safety parameters.

高碳材料转化为FG的估计能量：
Estimated energy for conversion of high carbon materials into FG:

对于100 mg批次，电容为60 mF的电容器组从220 V-150 V放电，然后
With 100 mg batch, a bank of capacitors with capacitance of 60 mF discharge from 220 V – 150 V, then

$$E = \frac{({V_1}^2 - {V_2}^2) \times C}{2 \times M} = 7.2\ kJ \cdot g^{-1}$$

E：每克所需能量
E: Energy per gram

V1和V2：分别为闪蒸前后的电压
V_1 and V_2: Voltage before and after flash, respectively

C：电容
C: Capacitance

M：每批质量
M: Mass per batch

拉曼光谱分析与涡轮层状石墨烯的讨论
Discussion of Raman Analyses and Turbostratic Graphene

石墨烯被定义为二维材料
Graphene is defined as a 2-D material

虽然石墨烯通常被描述为一层碳，但它仅在专门的实验室条件下作为一层孤立的碳。在我们这里报告的任何实质性生产方法中，石墨烯都将以聚集体的形式出现。该领域的先驱们将石墨烯定义为二维材料，而碳纳米管是一维材料，石墨是三维材料。当这些聚集体中的sp2碳片保留二维而非三维材料的电子结构时，则使用描述性形容词作为前缀，如双层石墨烯、少层石墨烯、N层石墨烯。如果AB堆叠(伯纳尔)，那么石墨烯是指厚度小于10层时使用的术语，因为相对于石墨，厚度小于10层时具有不同的物理性质。只有在>9层的情况下，才会出现类似石墨的特性，并且只有在相邻片层AB堆叠的情况下。当出现随机取向分层而不是像FG那样AB堆叠时，使用几个不同的形容词有相同的含义，例如：方向错误、扭曲、旋转、旋转故障、弱耦合、和涡轮层。

While graphene is often depicted as a single sheet of carbon, it occurs as a single isolated sheet only in specialized laboratory conditions. In any substantial production method such as we are reporting here, graphene will appear in the form of aggregates. The pioneers in this field have defined graphene as a 2-D material, in contrast to carbon nanotubes as a 1-D material and graphite as a 3-D material.[1, 2, 3, 4] When the sp^2-carbon sheets within these aggregates retain the electronic structure of a 2-D rather than 3-D material, then a descriptive adjective is used as a prefix, such as *bilayer graphene, few-layer graphene, N-layer graphene*. If AB-stacked (Bernal), then graphene is the term used when there are <10-layers since there are distinct physical properties, relative to graphite, at <10 layers. Only at >9 layers, do graphite-like property ensue and only if the adjacent sheets are AB-stacked.[5] When randomly oriented layering occurs rather than AB-stacked as in the case of FG, several different adjectives are used with the same meaning, such as: *misoriented*,[3] *twisted*,[6] *rotated*,[7] *rotationally faulted*,[8, 9] *weakly coupled*,[10] and

尽管术语各不相同，但许多作者一致认为，在这些情况下，各层在随机堆叠时仍保留其二维特性。
turbostratic.[11] In spite of the varied terminology, there is agreement among many authors that in
因此，科学
these cases, the individual layers retain their 2-D properties when randomly stacked. Hence, the
文献支持使用术语“ 石墨烯 ”进行此类堆叠，即使存在许多层。
use of the term "*graphene*" for such stacking is supported in the scientific literature, even when
正如我们将要展示的，拉曼光谱提供了对电子结构的直接监测，并且在表征这些
there are many layers.[12] As we will show, the Raman spectrum provides a direct monitor for the
聚集体的二维性质方面也很明确。
electronic structure and is also unambiguous in identifying the 2-D nature of these aggregates.

构成二维材料的不是物理尺寸或原子层数，而是特性，尤其是电子特性。
It is not the physical dimensions or the number of atomic layers but rather the properties,
石墨烯以狄拉克费米子的二维气体为特征。
especially electronic properties that constitute a 2-D material. Graphene is characterized by a 2-
二维材料是电子迁移率高度各向异性的材料，正如碳纳米管是一维材料一样，因
D gas of Dirac fermions.[13] A 2-D material is that which is highly anisotropic in electron mobility,
为在一个方向上的迁移率很高。
对于石墨烯，
just as carbon nanotubes are a 1-D material because high mobility in one direction. For graphene,
迁移率在x-y平面上是弹道式的，但当堆叠时，c轴迁移率要小得多。
the mobilities are ballistic in the x-y plane, but when stacked, the c-axis mobility is very much
涡轮层状石墨烯具有最大的各向异性，即使是多层石墨烯，其在二维中仍保持完全二维的弹
smaller. And turbostratic graphene has the greatest anisotropy of all, and even for multiple
道迁移率，在三维中电导率低很多数量级。
layers, it remains fully 2D with ballistic mobility in two dimensions, and many orders of
magnitude lower conductivity in the third dimension.

Kim等人的实验测量表明，当石墨烯片以扭曲的方式堆叠时，平面内的弹道电子和试图在
Experimental measurements by Kim et al. demonstrate that the extremely large
层间穿过的电子之间保留了极大的各向异性。
anisotropy between ballistic electrons in plane and those trying to cross between layers is
他们报告高度有序热解石墨
retained when the graphene sheets are stacked in a twisted manner.[7] They report $\sim 10^{-3}$ ohm-
(HOPG)的电阻约为10-3欧姆，比铜的电阻高约5个数量级，层间电阻又大4个数量级。
meter resistivity for highly ordered pyrolytic graphite (HOPG) which is ~5 orders of magnitude
higher resistivity than copper and the interlayer resistivity is again 4 orders of magnitude larger.
涡轮层状石墨烯的面内输运对于电子来说仍然是弹道式的。
涡轮层状石墨
The in-plane transport for turbostratic graphene remains ballistic for the electrons. Turbostratic
烯，即使有许多层，也是一种真正的二维材料，其中电子在二维中像无质量的费米气体一样自由移动，但实际
graphene, even with many layers, is truly a 2-D material whereby electrons move with complete
上无法垂直于层移动。
freedom like a massless Fermi gas in two dimensions but are, in effect, unable to move
很难找到像多层涡轮层状石墨烯这样纯二维的材料。
perpendicular to the layering. It is rare to find any other material that is so purely 2D as
multilayer turbostratic graphene.

拉曼光谱作为二维特征的最终标准

Raman as a definitive standard for 2-D character

拉曼光谱已成为诊断石墨烯的标准；这种工具几乎出现在每一项实验研究中。

Raman spectroscopy has become the standard as a diagnostic of graphene; that tool appears in almost every experimental study.[4, 7, 8, 9, 12, 14, 15, 16, 17] 这是因为它是石墨烯电子能带结构的直接探测器，而石墨烯的电子能带结构又在这种二维材料的独特特性中起着核心作用。And that is because it is a direct probe of the electronic band structure of the graphene, which in turn plays a central role in the unique character of this 2-D material.

涡轮层石墨与涡轮层石墨烯

Turbostratic graphite vs. turbostratic graphene

涡轮层状石墨的D峰远大于G峰和2D峰，这与FG的优化样品相反，FG的D峰远小于G峰，而G峰又小于2D峰。

The D-peak of turbostratic graphite is much larger than both the G-peak and the 2D peak, which is opposite for an optimized sample of FG which has a D-peak that is very much smaller than the G-peak, which in turn is smaller than the 2D peak.[18] 拉曼光谱是原子结构振动运动的探测器，因此巨大的D峰证明了涡轮层状石墨中单个石墨烯晶格被严重破坏。Raman spectroscopy is a probe of the vibrational motions of the atomic structure, hence the huge D-peak proves that the individual graphene lattice is very disrupted in turbostratic graphite. 它在纳米尺度上是非常无序的。It is profoundly disordered on the nanoscale. 它不能再还原为二维石墨烯材料。It can no more be restored to a 2-D graphene material. 研究人员对涡轮层状石墨烯这一非常有前景的领域的研究进展缓慢表示遗憾，因为很难获得这种材料。Researchers have lamented the slow development of the field of research into the very promising area of turbostratic graphene due to the difficulty of obtaining the material.[8, 11] 涡轮层状石墨烯仅通过CVD或外延生长产生微量(按重量计)。Turbostratic graphene was only produced in trace amounts (by weight) by CVD or epitaxial growth. 即使在这些精心控制的生长条件下生长，也不能保证材料是涡轮层状的。And even growth under these carefully controlled growth conditions, it does not assure that the material will be turbostratic. 有一组人尝试在镍箔上使用CVD制备10层涡轮层石墨烯，获得了不同的结果，有时是AB堆叠，有时是涡轮层，有时是两者的混合物。One group that attempted a thickness of 10-layer turbostratic graphene using CVD on nickel foil obtained varying results, sometimes AB-stacked, sometimes turbostratic, and sometimes a mixture of the two.[9] 即使是最近开发的涡轮层状石墨烯多层生长工艺也很难可靠。Even this recently developed process to multilayer growth of turbostratic graphene has been difficult to make reliable.

层数不定义二维特征
Number of layers does not define 2-D character

几位作者报道，对于AB堆叠石墨烯，单层石墨烯(SLG)或少层石墨烯(FLG)的二维性质逐渐转
Several authors have reported that for AB-stacked graphene, the 2-D properties of single-
变为三维材料，拉曼光谱在大约10层处演变为HOPG的特征。
layer graphene (SLG) or few-layer graphene (FLG) gradually transition to 3-D material with the
然而，这一经验
Raman spectra evolving into that characteristic of HOPG at about 10 layers.[3, 13] However, this
法则不适用于涡轮层状石墨烯，因为各个层是弱耦合的，因此它们保留了与层数无关的二维特征。
rule of thumb does not apply to turbostratic graphene because the individual layers are weakly
2D峰保
coupled, so they retain the 2-D character independent of the number of stacked layers.[7, 9] The 2D
留其狭窄的洛伦兹线型，并且在K点处没有向Dirac锥引入额外的状态。
peak retains its narrow Lorentzian lineshape, and no additional states are introduced to the Dirac
因此，2D峰的拉曼散射仍然是一个单峰，该单峰具有双重共振增强，从而导致其强
cone at the K-point. Hence the Raman scattering for the 2D peak remains a single peak that is
烈增强。
它仍然是零带隙半导体。
doubly resonance enhanced, giving rise to its strong enhancement. And it remains a zero band
相反，当两层AB堆叠时，强耦合会在K点周围创建抛物线形状的附加状态，从而允
gap semiconductor. In contrast, when two layers are AB-stacked, the strong coupling creates
许更多的跃迁。
additional states with a parabolic shape around the K-point, which allows for more transitions.
2D峰由四个洛伦兹峰(两个强峰和两个弱峰)组成，在失去洛伦兹线形状的同时大幅加宽。
The 2D peak becomes a sum of four Lorentizians, two strong and two weak, and it substantially
几位作者研究了旋转取向错误的石墨烯，有些
broadens while losing its Lorentzian line shape. Several authors have studied rotationally
人通过折叠单张的方法来保证错位。
misoriented graphene, some by the method of folding a single sheet, which guarantees
由于2p原子轨道重叠不良，两个薄片保留了其SLG特性。
misalignment. As a result of the poor overlap of the 2p atomic orbitals, the two sheets retain
their SLG characteristics.[7, 9, 11]

存在或不存在某些相对较弱的拉曼组合带是涡轮层石墨烯出现的积极指标：1650 cm -1至2300 cm -1
The presence or absence of certain relative weak Raman combination bands are positive
波数范围内生长石墨烯的组合拉曼模式以及拉曼2D模式的特征被用作涡轮层石墨烯的特征。
indicators for the occurrence of turbostratic graphene: “Combination Raman modes of as-grown
graphene within the frequency range of 1650 cm^{-1} to 2300 cm^{-1}, along with features of the
有一个
Raman 2D mode, were employed as signatures of turbostratic graphene.” There is a
平面内横向声学(iTA)和纵向光学(LO)、iTA和纵向声学(LA)以及LO+LA模式的组合。
“combination of in-plane transverse acoustic (iTA) and the longitudinal optic (LO), iTA and
在这里，我们将iTALO模式指定为TS1，将
longitudinal acoustic (LA) and LO + LA modes. Here, we designate the iTALO− mode as TS_1
iTOLA/LOLA模式指定为TS2。
and the iTOLA/LOLA modes as TS_2.”[11]

使用TS1和TS2作为正面指标

Using TS_1 and TS_2 as positive indicators

我们将使用TS1和TS2的名称来表示这两个仅对SLG和涡轮层石墨烯具有拉曼活性的特征。 TS1是发生在1880 cm -1附近的单个洛伦兹，TS2由发生在2030 cm -1附近的两个紧密空间洛伦兹组成；然而，必须记住，这些谱线表现出色散，就像石墨烯中的许多拉曼特征一样。 必须始终注意激发波长，并在比较峰值频率时应用色散校正。

We will use the designations of TS_1 and TS_2 to indicate these two features that are Raman active only for SLG and turbostratic graphene. TS_1 is a single Lorentzian that occurs in the vicinity of 1880 cm^{-1} and TS_2 consists of two closely space Lorentzians that occurs in the vicinity of 2030 cm^{-1}; however, it must be kept in mind that these lines exhibit dispersion, like many Raman features in graphene. The excitation wavelength must always be noted, and dispersion corrections applied when comparing the peak frequencies.

消失的M带

The silent M band

此外，“ M ”带出现在1750 cm-1左右，但对于涡轮层状石墨烯，该组合带变得消失。 因此，M带的存在是涡轮层状石墨烯的负指标，也是AB堆叠石墨烯和HOPG的正指标。

In addition, the "M" band occurs about 1750 cm^{-1} but this combination band becomes silent for turbostratic graphene. Hence the presence of the M band is a negative indicator for turbostratic graphene, and a positive indicator for AB-stacked graphene as well as HOPG.

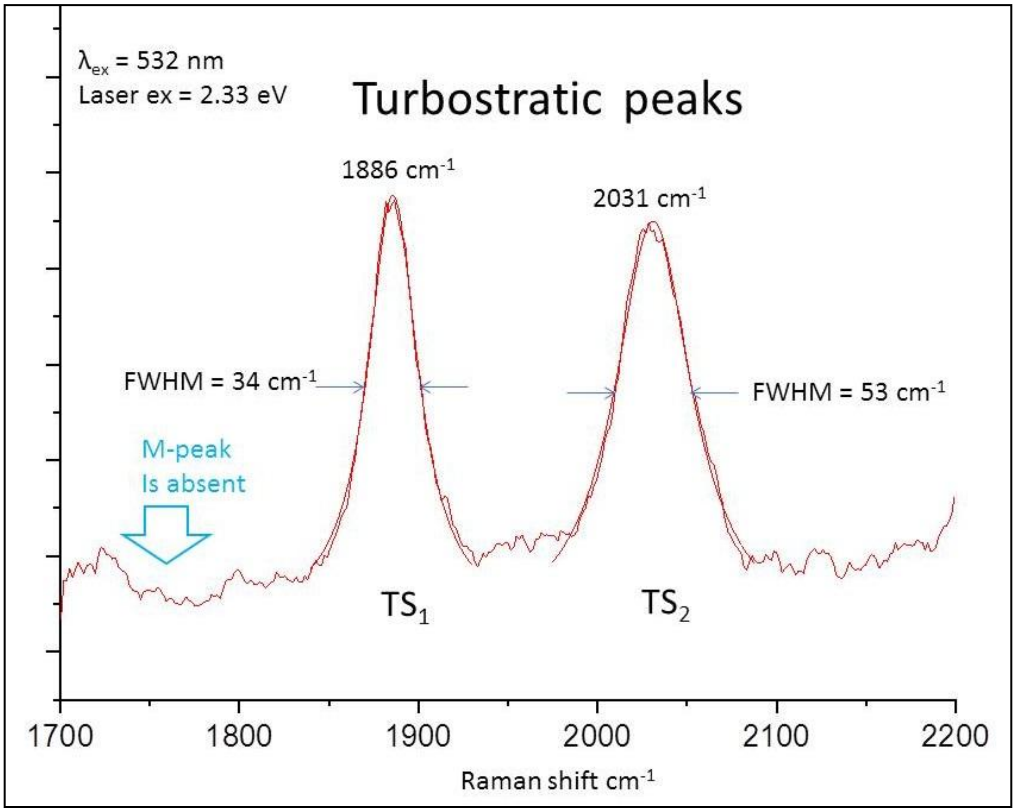

补充图2. CB-FG拉曼光谱中的涡轮层峰。
Supplementary Fig. 2. Turbostratic peaks in the Raman spectrum of CB-FG. $I_{G/TS1}$ ~30.
洛伦兹拟合显示为叠加的平滑线。 对于TS1，R平方为0.994，对于TS2，R平方为0.99。
Lorentzian fit is shown as a superimposed smooth line. The R-squared is 0.994 for TS_1 and 0.99 for TS_2.
这些极好的拟合表明FG的高质量，并且这些拉曼谱线的明显存在可归因于涡轮层状石墨烯。
These excellent fits indicate the high quality of the FG and the unmistakable presence of these Raman lines are attributable to turbostratic graphene.

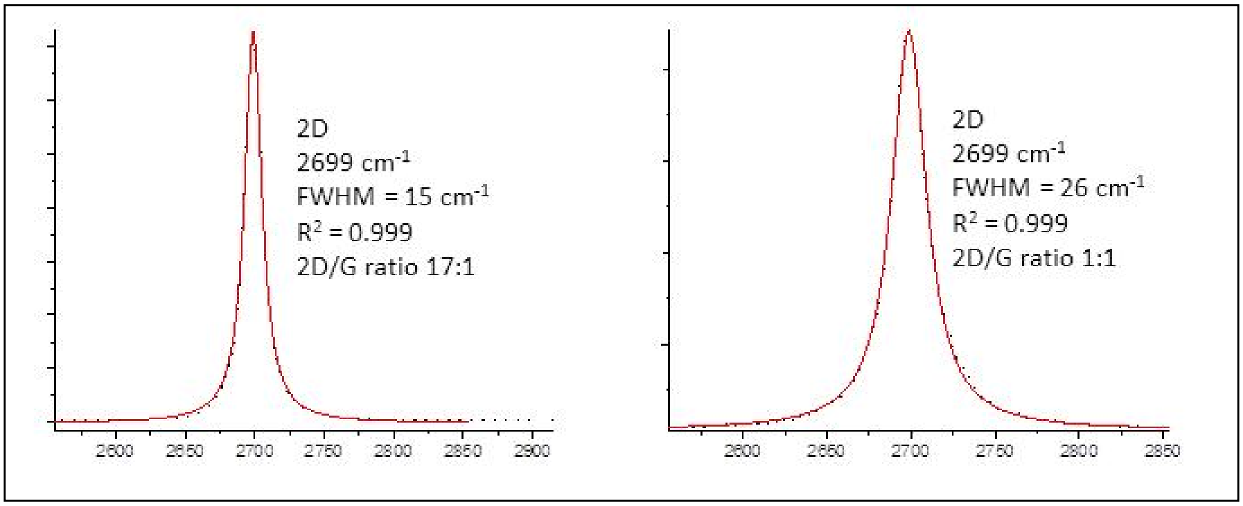

补充图3. CB-FG拉曼光谱中的2D峰。 左：CB-FG中的最佳点,
Supplementary Fig. 3. 2D peak in the Raman spectrum of CB-FG. Left: best point in CB-FG,
右：CB-FG中的代表点。 两个峰都呈现出近乎完美的洛伦兹线型。
right: representative point in CB-FG. Both peaks exhibit nearly a perfect Lorentzian line shape.
黑点是理论上的线形。 两个峰值的相关性R2均为0.999。
The black dots are the theoretical line shape. The R^2 for the correlation is 0.999 for both peaks.
这表明K点处有一个完全锥形的狄拉克锥。 超大的I2D/G也表明了多层涡轮层
This is indicative of a fully conical Dirac cone at the K-point. The exceptionally large $I_{2D/G}$ is
石墨烯，因为一些研究人员指出
also indicative of multilayer turbostratic graphene, as several researchers point to an increasing $I_{2D/G}$.[7, 11]

狭窄的单洛伦兹2D峰只能出现在SLG或涡轮层状石墨烯中，相邻层被解耦，不会产生额外的电子态。
The narrow, single Lorentzian 2D peak can occur only for either SLG or turbostratic graphene whereby the adjacent layers are decoupled and do not give rise to additional electronic
这反过来意味着它仍然是完美的二维，即使有许多层石墨烯堆叠。
states. This in turn means that it remains perfectly 2-dimensional, even though there are many
对于图3左侧的最佳示例，洛伦兹半最大全宽(FWHM)实际上比理想SLG更窄。
layers of graphene stacked. For the best example on the left of Fig. 3, the Lorentzian full-width-at-half-maximum (FWHM) has actually become narrower than for the perfect SLG. This
这种变窄是旋转错位石墨烯的一个独特特征，这种石墨烯是堆叠的，并且只发生在涡轮层压石墨烯上，如下所述，
narrowing is a unique feature of rotationally misaligned graphene that is stacked and only occurs
与其他报告相比。 我们观察到2D峰窄至15 cm-1,
for turbostratic graphene, as describe below relative to other reports. We have observed 2D peaks
这仅发生在多层涡轮层状石墨烯中。 更宽的谱带
as narrow as 15 cm^{-1}, which occurs only for multiple layers of turbostratic graphene. The much
是伯纳尔双分子层，它是四个峰的总和，显然不是洛伦兹的。
broader band is for a Bernal bilayer, which is a sum of four peaks and is clearly non-Lorentzian.

CB-FG与已报道的涡轮层状石墨烯拉曼光谱的比较
Comparison of the Raman spectrum of CB-FG to those in reported turbostratic graphene

补充表1:2D、TS1和TS2峰值与之前研究的比较。
Supplementary Table 1: Comparison of 2D, TS_1 and TS_2 peak with previous studies. The
这个对先前使用514 nm激发激光的研究中的峰值位置进行了校正，以匹配本研究中的532 nm激发激光。
peak position from previous studies that used 514 nm excitation laser are corrected to match the 532 nm excitation laser in this study.

	2D		TS_1		TS_2	
	Position	FWHM	Position	FWHM	Position	FWHM
Niilisk *et al.*[9]	2697	36	1886	34	2030	54
Garlow *et al.*[11]	2702	27	1884	38	2031	51
CB-FG	2699	15-26	1886	34	2031	53

将CB-FG光谱与来自两个不同参考文献的数据进行比较，发现
Comparing CB-FG spectra with data from two different references, the locations and
两种情况下，两个TS(涡轮层流)峰值的FWHM基本相同。 2D峰的位置也相
FWHM of the two TS (turbostratic) peaks are essentially identical in both cases. The location of
同，CB-FG洛伦兹峰与Garlow等人的较窄FWHM相匹配。
the 2D peak is also the same, with the CB-FG Lorentzian matching the narrower FWHM in that
我们观察到2D峰窄至15 cm-1，这仅发生在多层涡轮层状石墨烯中。
from Garlow *et al.* We have observed 2D peaks as narrow as 15 cm^{-1}, which occurs only for
与Niilisk等人相比，Niilisk等人有多达6层涡轮层状石墨烯，
multiple layers of turbostratic graphene. Comparing to Niilisk *et al.*, which has up to 6 layers of
同样在频率和宽度上与TS1和TS2峰几乎相同。
turbostratic graphene, again there is a near identical match with the TS_1 and TS_2 peaks both in
对于参考文献和我们的CB-FG，均不存在AB堆叠石墨烯和HOPG的特征M峰。
frequency and width. And for both references and our CB-FG, the M-peak which is
因此，涡轮层CB-FG拉曼数据与
characteristic of both AB-stacked graphene and HOPG, is absent. Therefore, there are several
从已证实的涡轮层石墨烯获得拉曼光谱的两个参考文献之间存在若干精确和冗余的光谱特征比对。
precise and redundant spectral feature alignments between the turbostratic CB-FG Raman data and two references that have obtained Raman spectra from proven turbostratic graphene. In
此外，二维洛伦兹FWHM的变窄进一步支持了涡轮层流叠加作为二维材料。
addition, the narrowing of the 2D Lorentzian FWHM is further support of the turbostratic stacking as a 2-D material.

非常小的D带
The very small D-band

有趣的是，并非所有边缘都表现为缺陷；因此，它们并不总是显示D波段。
Interestingly, not all edges behave as defects; hence they will not always display a D-band. For
对于锯齿形边缘，产生D带的声子保持消失。 由于锯齿边缘是自由生长石
the zigzag edge, the phonon that gives rise to the D-band remains silent. Since the zigzag edge is
墨烯最可能的边缘，因此边缘的声子可以保持消失，因此观察到的D带仍然很小。
the most probable edge for freely growing graphene then that phonon for the edges can remain
当Yan等人对他们的大六方单晶石墨烯进行了
silent, thus the D-band remains very small as observed. This was experimentally verified when
彻底的拉曼图谱时，实验证实了这一点，并且D带在边缘仍然很小。
Yan et al. did a thorough Raman map of their large hexagonal single-crystal graphene and the D-band remained very small at the edges.[19]

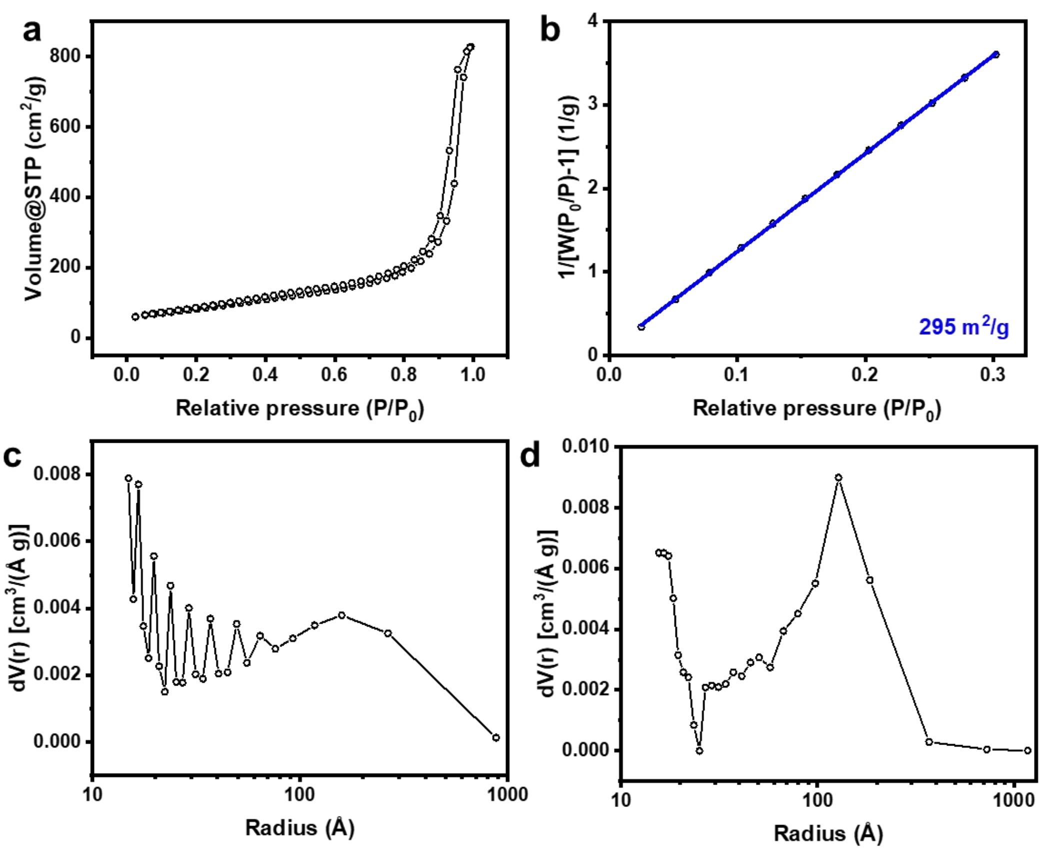

补充图4。CB-FG的BET表面积分析。 等温线。 BET表面积
Supplementary Fig. 4. **BET surface area analysis of CB-FG.** a. Isotherm. b. BET surface area
拟合 吸附和解吸孔径分布。
fitting. c-d. Absorption and desorption pore size distribution.

补充表2：图1中各种材料的FJH参数。持续时间是开关打开时间，而不是真正的闪蒸持续时间。
Supplementary Table 2: FJH parameters for various materials in Fig. 1. Duration is the switch
电压行中的蓝色表示没有闪蒸的预处理，红色表示FG合成
opening time, not the real flash duration. Blue colors in the voltage row signify pre-treatment
期间的实际闪蒸。 预处理是将材料部分炭化，
without a flash, red colors signify an actual flash during the FG synthesis. The pre-treatment is to
以减少挥发性材料并增加电导率。
partially char the material to reduce the volatile material and increase the conductivity. The
通过拉曼分析，炭化过程仅提供非晶态材料。 这种预处理对于低碳含
charring process affords only amorphous material by Raman analysis. This pre-treatment is
量的起始材料至关重要。 这种预炭化可以通过选矿材料来避免，其中有
crucial for starting materials with low carbon content. This pre-charring can be obviated with a
一个预热循环，因为当加热温度低于一定温度时，工业加热比用电加热便宜。
beneficiation material wherein there is a pre-heat cycle since industrial heating is less expensive
我们还列出了一种选矿材料，橡胶
than using electricity when heating below certain temperatures. And we also list a beneficiation
轮胎衍生炭黑，在工业上去除了挥发分，留下了碳残渣（见橡胶材料一节）。
material, rubber tire-derived carbon black, where the volatiles were industrially removed, leaving
a carbon residue (see the rubber materials section).

起始材料 **Starting material**	重量 **Weight (mg)**	管 **Tube** （毫米） **(mm)**	电容 **Capacitance (mF)**	电阻 **Resistance (Ω)**	电压 **Voltage** 预处理 **Pretreat** 闪蒸 **Flash**	持续时间 **Duration** （毫秒） **(ms)**	生产的材料 **Result material**
炭黑（黑珍珠 Carbon black 2000，卡博特 (Black Pearls ） 2000, Cabot)	30	4	60	1.5	35 V x 5 110 V	500 50	CB-FG（最高 CB-FG (highest $I_{2D/G}$)
	120	8	60	1	60 V x 5 220 V	500 500	CB-FG（塑料复 CB-FG (plastic 合） compounding)
	1200	15	220	1.5	100 V x 5 250 V	500 500	CB-FG（1.1 CB-FG (1.1 g g批次） batch)
用过的咖啡 Used coffee 渣/CB grounds/ CB	1000	10	220	1000-3000 150 V x 3 10000焦咖啡渣 1000-3000	150 V x 3	10000	Charred coffee grounds

(5%) (星巴克和 (Starbucks and 折叠器) Folgers)							
烧焦的咖啡渣 Charred coffee grounds	50	4	60	5-10	40 V x 5 130 V	50	C-FG
无烟煤 Anthracitic coal (费希尔科学公司 (Fisher Scientific S98806)	80	4	60	2000-3000 150 V 10000无烟煤衍生 2000-3000	150 V	10000	Anthracite-derived FG
煅烧焦炭 Calcine coke (牛轭 (Oxbow 煅烧 Calcining 国际，CPC International, 1400) CPC 1400)	80	4	60	0.8	80 V x 5 175 V	100 500	煅烧焦化FG Calcined coke-derived FG

闪蒸石墨烯形态

Flash Graphene Morphology

大多数有机化合物在高温退火时会石墨化。
Most organic compounds will graphitize when annealed at elevated temperature. During
在石墨化过程中，有机材料被加热，通过热解增加碳含量。
the graphitization process, an organic material is heated, increasing carbon content via pyrolysis.
在热解过程中，碳与相邻的碳原子形成sp2杂化共价键，并结晶成石墨的层状区域。
During pyrolysis, the carbon forms sp^2-hybridized covalent bonds with neighboring carbon
非碳元素在极端温度下挥发。
atoms and crystallizes into layered domains of graphite. Non-carbon elements volatilize at the
然而，石墨化材料的结构在很大程度上取决于制备方法以及起始材料。
extreme temperatures. However, the structure of graphitized material largely depends upon the
罗莎琳德·富兰克林(
method of preparation as well as the starting material. Some of the earliest work to critically
Rosalind Franklin)最早对碳石墨化的各种形态进行了批判性综述
comment on the various morphologies of carbon graphitization was that of Rosalind Franklin,[20]

它纯粹通过X射线衍射和密度测量来研究形貌。
which studied morphologies purely by means of x-ray diffraction and density measurements. It
人们注意到，将几个非石墨碳加热到1700到3000 ° C之间后，sp2杂化碳层将定向为相对致密的结晶石墨。
was noted that after heating several non-graphitic carbons to temperature between 1700 and
3000 °C, layers of sp^2-hybridized carbon would orient into relatively dense crystalline graphite.
这些被称为石墨化碳。 其他碳起始材料在退火时会形成平行组的多孔石墨层，而
These were termed *graphitizing carbons*. Other carbon starting materials would form porous
不会沿c轴扩展堆叠。
graphite-like layers in parallel groups when annealed, without extended stacking along the c-axis.
这些被称为非石墨化碳。
These were termed as *non-graphitizing carbons.*

随着原子分辨显微镜技术的出现，石墨化和非石墨化碳的结构可以可视化，以进一步揭示其形态。
With the advent of atomic resolution microscopy techniques, the structure of *graphitizing*
and *non-graphitizing carbons* could be visualized to further reveal their morphologies. High
高分辨率TEM图像显示，非石墨化碳，如聚偏二氯乙烯和炭黑，可能形成封闭的碳纳米颗粒，其结构类似富
resolution TEM images have shown that non-graphitizing carbons, such as polyvinylidene
勒烯，类似于正文3d中报告的闪蒸石墨烯的模拟结构。
chloride and carbon black, may form closed carbon nanoparticles which are fullerene-like in
structure,[21] and resemble the simulated structure of flash graphene reported in Figure 3d of the
这些粒子的特征是沿所有侧面的晶格条纹，这表明是一种三维富勒烯样结构。
manuscript. These particles are characterized by lattice fringes along all sides, which suggest a 3-
Iijima的研究表明，石墨化炭黑可以形成类似富勒烯的多面体，其厚度
D fullerene-like structure. Work by Iijima reveals that graphitized carbon black can form
为单层到几层。 这些被命名
fullerene-like polyhedra of carbon which are single to few layers in thickness.[22] These were
为石墨烯多面体。 这些结构的特征是沿石墨烯多面体边缘约120±20o的角度，表明存在弯曲所需
named graphene polyhedra. These structures are characterized by angles of ~ 120 ± 20^o along the
的一些5-7个成员环。
edge of the graphene polyhedra and suggest the presence of some 5-7 member rings required for
后来，Dresselhaus等人在透射电子显微镜中通过焦耳加热观察到非晶碳的实时石墨化。
bending. Later, Dresselhaus et al. observed the real-time graphitization of amorphous carbon
特别有趣的是，在焦耳加热时观察到石
via Joule heating in a transmission electron microscope.[23] Of particular interest, formation of
墨烯多面体粒子的形成，石墨壳层的厚度随着退火时间的增加而增加。
graphene polyhedra particles are observed upon Joule heating, with the thickness of the graphitic
Wang等人的其他研究表明，碳纳米纤维的电石墨化和剥离可以得
shell increasing with annealing time. Other work by Wang et al. demonstrated that the electro-
到石墨烯。 24然而，拉曼分析显
graphitization and exfoliation of carbon nanofibers can be afford graphene.[24] However, Raman
示，通过电石墨化，石墨烯的质量相对较差。
analysis reveals a relatively poor quality of graphene by electrographitization.

在这项工作中，可以发现石墨烯的各种形态，从石墨烯薄片到石墨烯多面体，如正文的图1所示。
In this work, various morphologies of graphene can be found ranging from sheets of
这些形态在很大程度上
graphene to graphene polyhedra, as shown in Figure 1 of the manuscript. These morphologies
取决于碳起始材料，它反映了起始材料是石墨化碳还是非石墨化碳；然而，对于FG工艺而言，加热和冷却的时
largely depend upon the carbon starting material which reflects whether the starting material is a
间尺度为毫秒。
graphitizing or *non-graphitizing* carbon; however, unique to the FG process, heating and cooling
快速的加热和冷却速度阻止了石墨烯层的堆叠形成石墨，也
occurs over the timescale of milliseconds. Fast heating and cooling rates prevent the stacking of
阻止了石墨烯层的旋转注册，从而形成涡轮层叠石墨烯。
graphene layers to form graphite, and it also prevents the rotational registration of graphene
这就产生了从光谱学上观察到的特殊石墨烯质量。
layers thus resulting in turbostratic graphene. This gives rise to the exceptional graphene quality
所有经过闪蒸的碳源至少显示出一些石墨烯多面体类型的形态。
observed spectroscopically. All carbon sources that were flashed exhibited at least some
正文中的图1显示，这项工作中的闪蒸石
morphologies which are of the graphene polyhedral type. Figure 1 from the manuscript shows
墨烯可以具有与文献中提到的多面体结构相似的多面体结构，多个边缘角范围为109-130°。
that flash graphene in this work can have a similar polyhedron structure to that mentioned in
多面体通常由<5层组成，构成FLG
literature with many edge angles ranging from 109 – 130°. The polyhedra are commonly
分类。 然而，当焦耳加热时，一些碳起始
composed of <5 layers which constitutes classification as FLG. However, some carbon starting
材料也会形成薄片。 补充表S2中总结了我们的闪蒸石墨烯
materials will also form sheets when Joule heated. A summary of our flash graphene
形态。虽然没有针对所有起始材料进行优化，但无烟煤、咖啡、生物炭、煅烧焦炭和松木等材料形成石墨烯片。
morphologies can be found in Supplementary Table S2. Though not optimized for all the starting
materials, materials such as anthracite coal, coffee, biochar, calcined coke, and pine form
这与我们的发现一致，即形成石墨烯片的所有FG碳源以前在文献报告中被归类为石墨化碳
graphene sheets. This is consistent with the finding that that all of our FG carbon sources which
（补充表S2）。
form graphene sheets have formerly been classified as *graphitizing carbon* in literature reports
因此，FG的最终形态在很大程度上取决于起始碳源。
(Supplementary Table S2). Hence, the resultant morphology of FG largely depends on the
被归类为石墨化碳的材料在热退火时很容易热解成石墨，通常在闪蒸时会部分形成
starting carbon source. Materials classified as *graphitizing carbons,* which will readily pyrolyze
石墨烯片。
into graphite when thermally annealed, generally result in the partial formation of graphene
石墨化和非石墨化碳材料都会在闪蒸过程中形成石墨烯多面体。
sheets when flashed. Materials classified as *graphitizing* and *non-graphitizing carbons* all result
这表明与FJH相关的快速加热和
in the formation of graphene polyhedra during the flashing process. This suggests that the rapid
冷却速度有效地阻止了晶体的进一步结晶
heating and cooling rates associated with FJH effectively retards further crystallization of the

石墨烯多面体转变为石墨畴，从而产生独特的结构，这种结构在炉加热的石墨化材料中通常不存在，这种材料
graphene polyhedra into graphitic domains, thereby giving rise to unique structures not typically
经历相对缓慢的加热和冷却。
found in furnace-heated graphitized material which undergo a relatively slow heating and
FG结构由超高纯度、低缺陷材料组成，这些材料可产生特殊的拉曼特征，例如I2D/G比高达17。
cooling. FG structures are composed of ultra-high purity, low defect material which give rise to exceptional Raman signatures, such as a $I_{2D/G}$ ratio of up to 17.

补充表3。表报告了从每个碳源形成闪蒸石墨烯时石墨烯多面体或石墨烯片的存在。
与文献比较
表明石墨化碳(已知在热解时形成石墨)导致石墨烯片的形成。
所有闪蒸材料都显示出一些石墨烯多面体。
Supplementary Table 3. Table reporting the presence of graphene polyhedra or graphene sheets when forming flash graphene from each carbon source. Comparison to literature shows that *graphitizing carbons* (which are known to form graphite upon pyrolysis) result in formation of graphene sheets. All flashed materials exhibit some graphene polyhedral.

碳源 **Carbon Source**	石墨烯多面体 **Graphene polyhedra**	石墨烯片 **Graphene sheets**	参考文献中的热解形态 **Pyrolysis morphology in references**
炭黑 Carbon black	Yes	No	热解形成石墨烯多面体 Pyrolysis forms graphene polyhedra[20, 25]
煅烧石油焦 Calcined petroleum coke	Yes	No	热解形成结晶石墨域 Pyrolysis forms crystalline graphite domains[20]
咖啡渣 Coffee grounds	一些来自炭黑导电掺杂剂 Some from CB conductive dopant	Yes	纤维素和木质素的热解形成结晶石墨域 Pyrolysis of cellulose and lignin forms crystalline graphite domains[26, 27]
无烟煤 Anthracite coal	一些来自CB掺杂剂是 Some from CB dopant	Yes	热解形成结晶石墨域 Pyrolysis forms crystalline graphite domains[20]

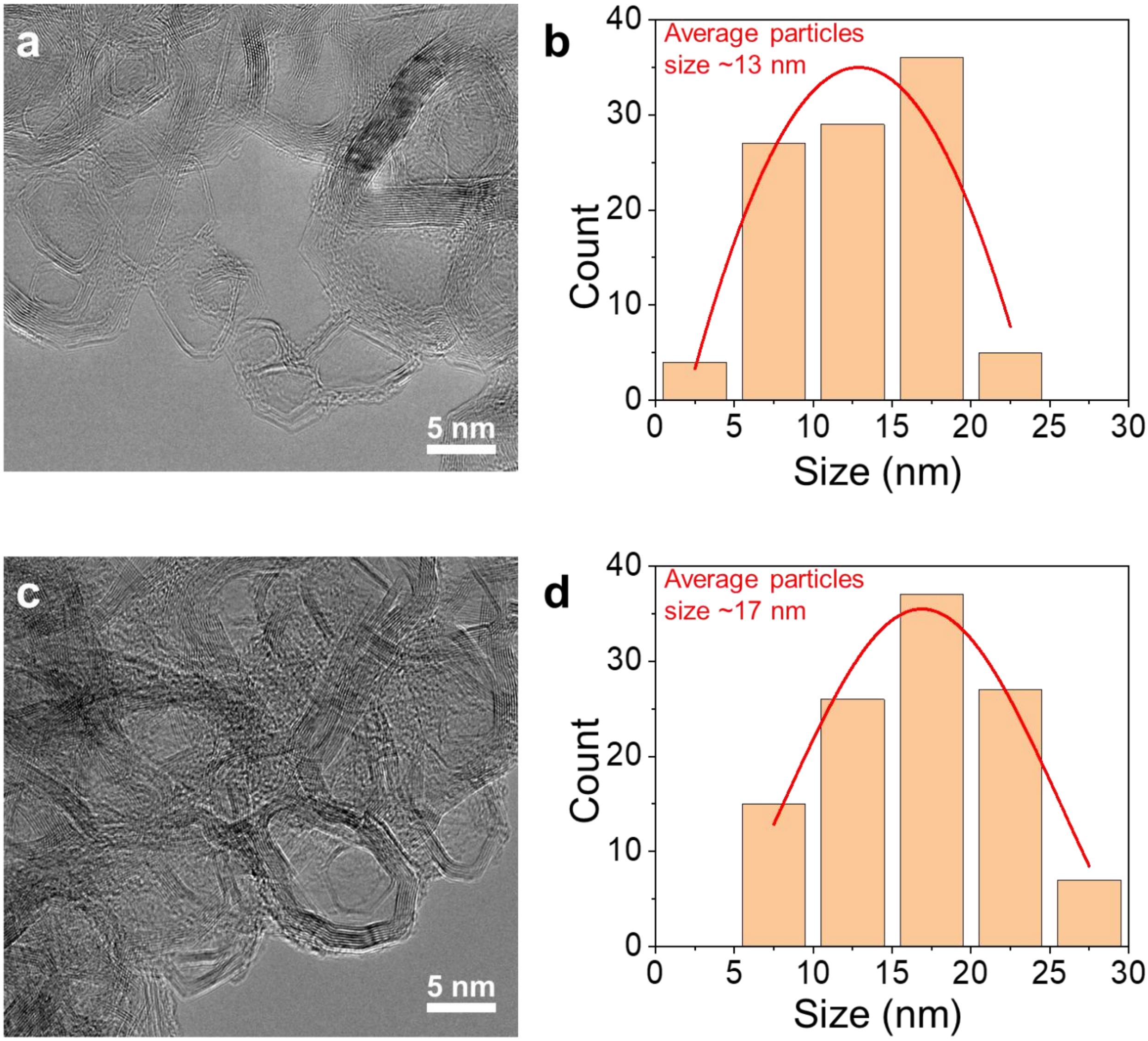

补充图5。CB-FG和CPC-FG的尺寸分布。 CB的HR-TEM图像-
Supplementary Fig. 5. **Size distribution of CB-FG and CPC-FG.** a. HR-TEM image of CB-
CB-FG尺寸分布直方图。 CPC-FG的HR-TEM图像。 CPC-FG尺寸
FG. b. Histogram for size distribution of CB-FG. c. HR-TEM image of CPC-FG. d. Histogram
分布直方图。
for size distribution of CPC-FG.

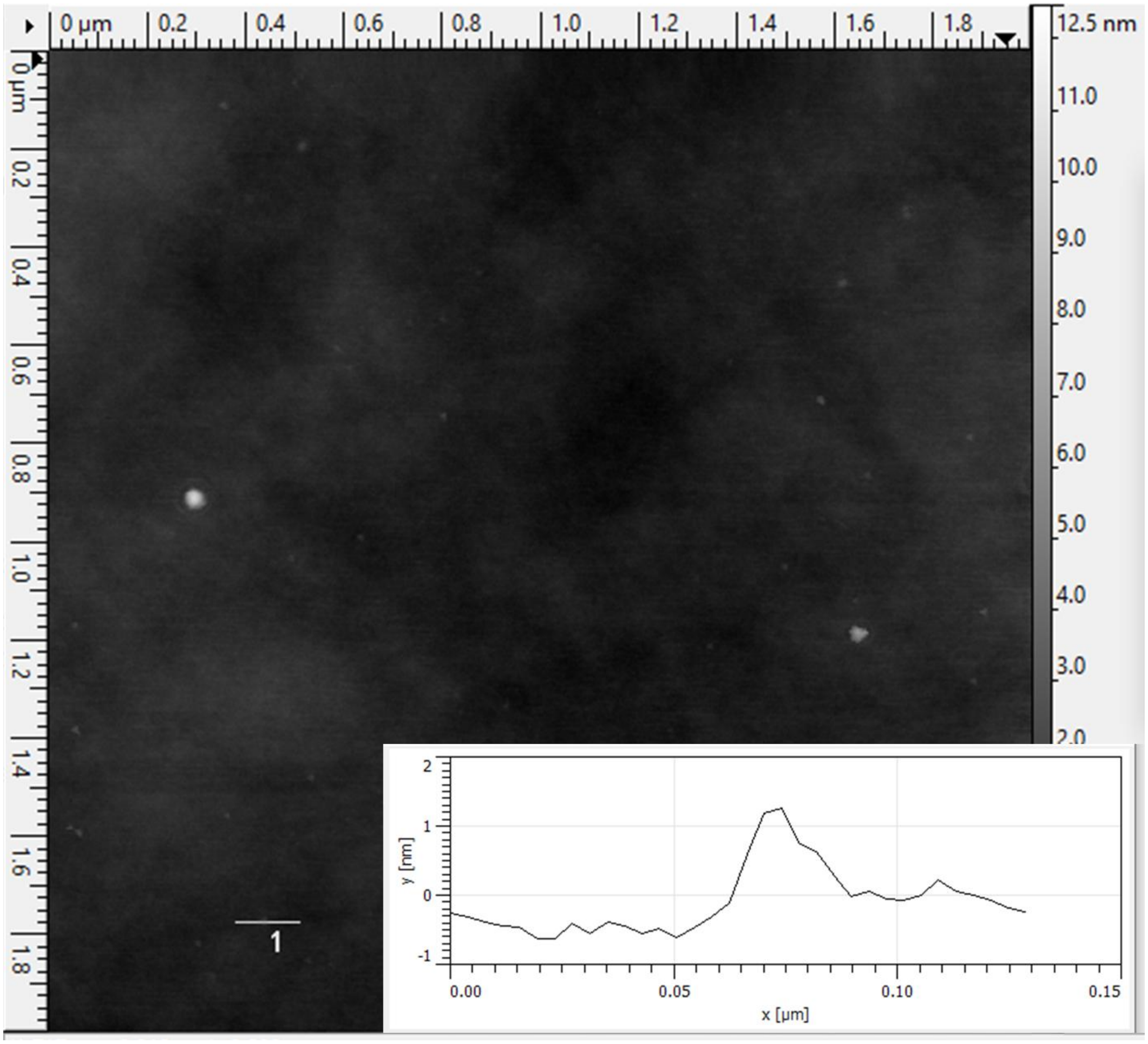

补充图6。炭黑衍生FG的AFM表征。
Supplementary Fig. 6. **AFM characterization of carbon black-derived FG.** CB-FG is
分散在N-甲基-2-吡咯烷酮(NMP)溶液中，并沉积在硅酮基底上。
dispersed in *N*-methyl-2-pyrrolidone (NMP) solution and deposited onto a silicone substrate. The
如补充图5所示，单个CB-FG颗粒位于表面上，高度约为1.2 nm，由FLG产生。
individual CB-FG particles as seen from Supplementary Fig. 5 lay on the surface with height of

~ 1.2 nm that result from FLG.

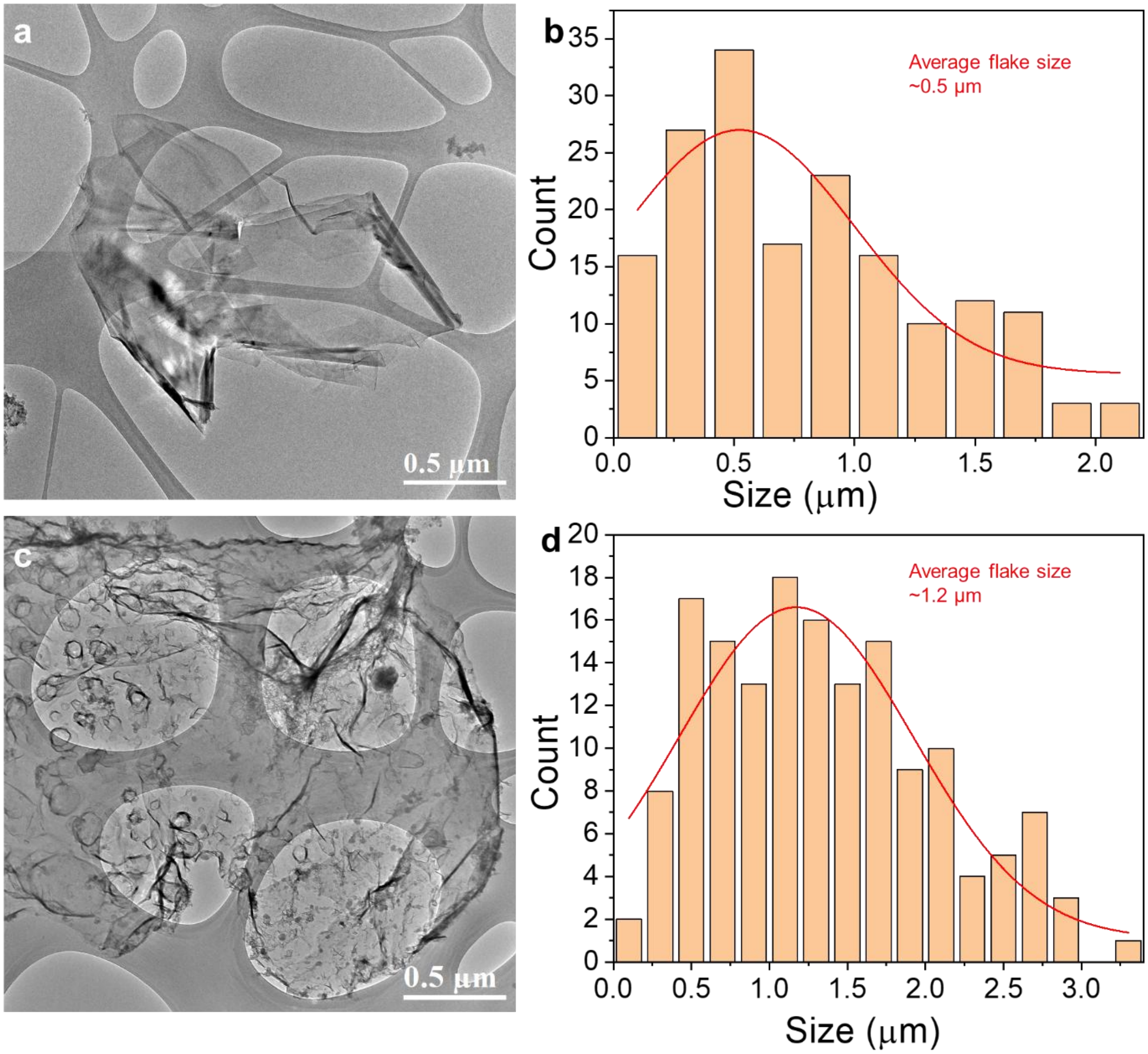

补充图7。无烟煤和咖啡衍生FG的粒度分布。
Supplementary Fig. 7. **Size distribution of anthracite- and coffee-derived FG.** a. HR-TEM

A-FG的图像。 A-FG尺寸分布直方图。 C-FG的HR-TEM图像。
image of A-FG. b. Histogram for size distribution of A-FG. c. HR-TEM image of C-FG. d.

C-FG尺寸分布直方图。
Histogram for size distribution of C-FG.

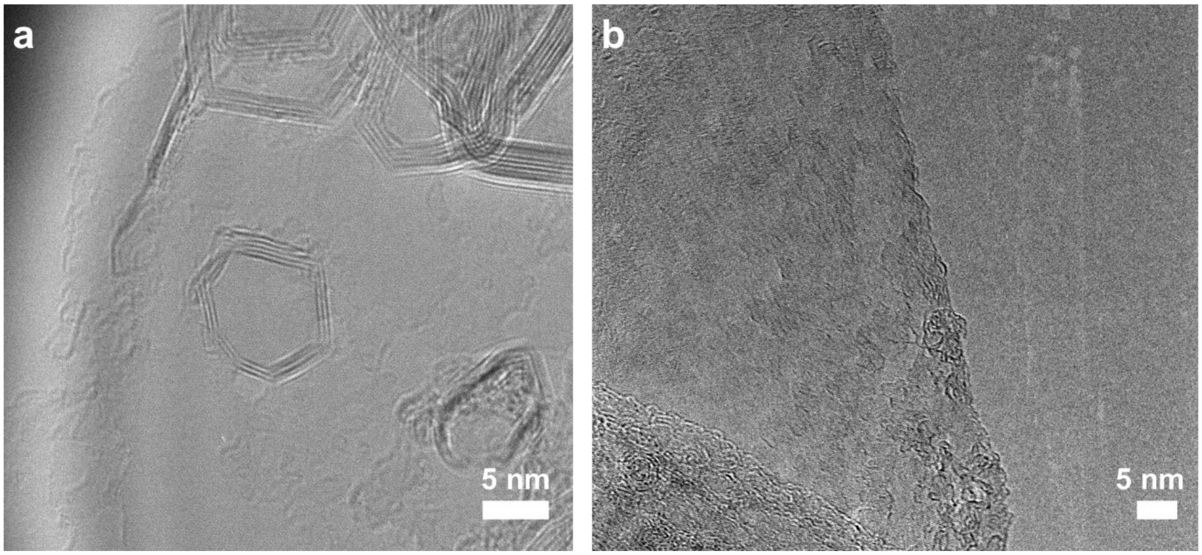

补充图8.（a）C-FG和（b）a-FG单层石墨烯的TEM图像。

Supplementary Fig. 8. TEM images of single layer of graphene from (a) C-FG and (b) A-FG.

CB-FG有一些多面体石墨烯，也可能来自用于增加FJH电导率的CB掺杂剂。

The CB-FG has some polyhedral graphene that could also come from the CB dopant used to increase the conductivity for FJH.

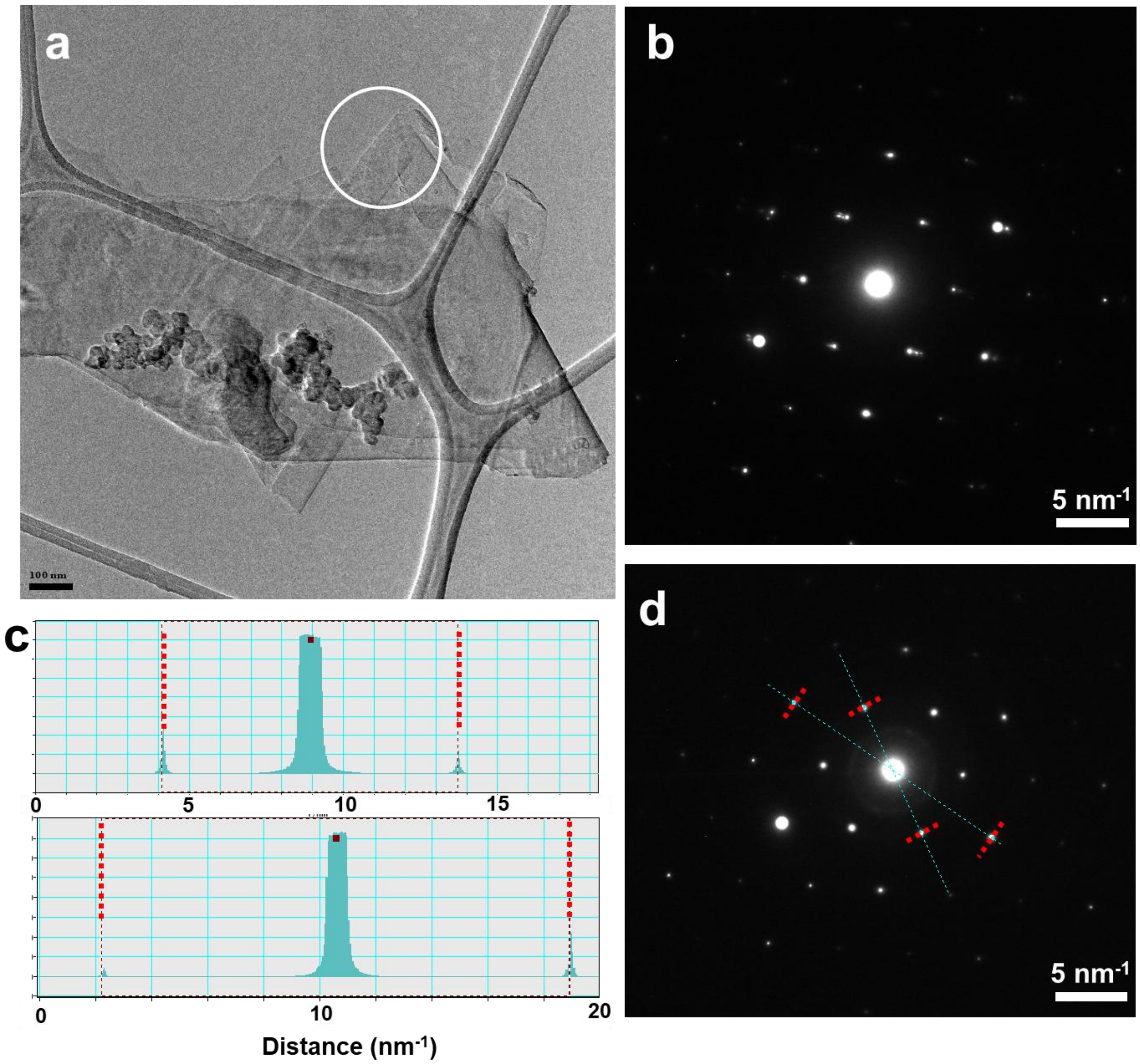

补充图9.无烟煤衍生FG的SAED。 a-FG薄片的TEM图像和
Supplementary Fig. 9. **SAED of anthracite-derived FG**. a. TEM image of a A-FG flake and
SAED的位置。 显示层间错位的几层石墨烯位置的SAED。
the position for SAED. b. SAED of the few-layer graphene position that shows misalignment
SLG的SAED与先前研究中的SLG相关。
between layers. c-d. SAED of SLG that correlates with SLG in previous studies.[28, 29]

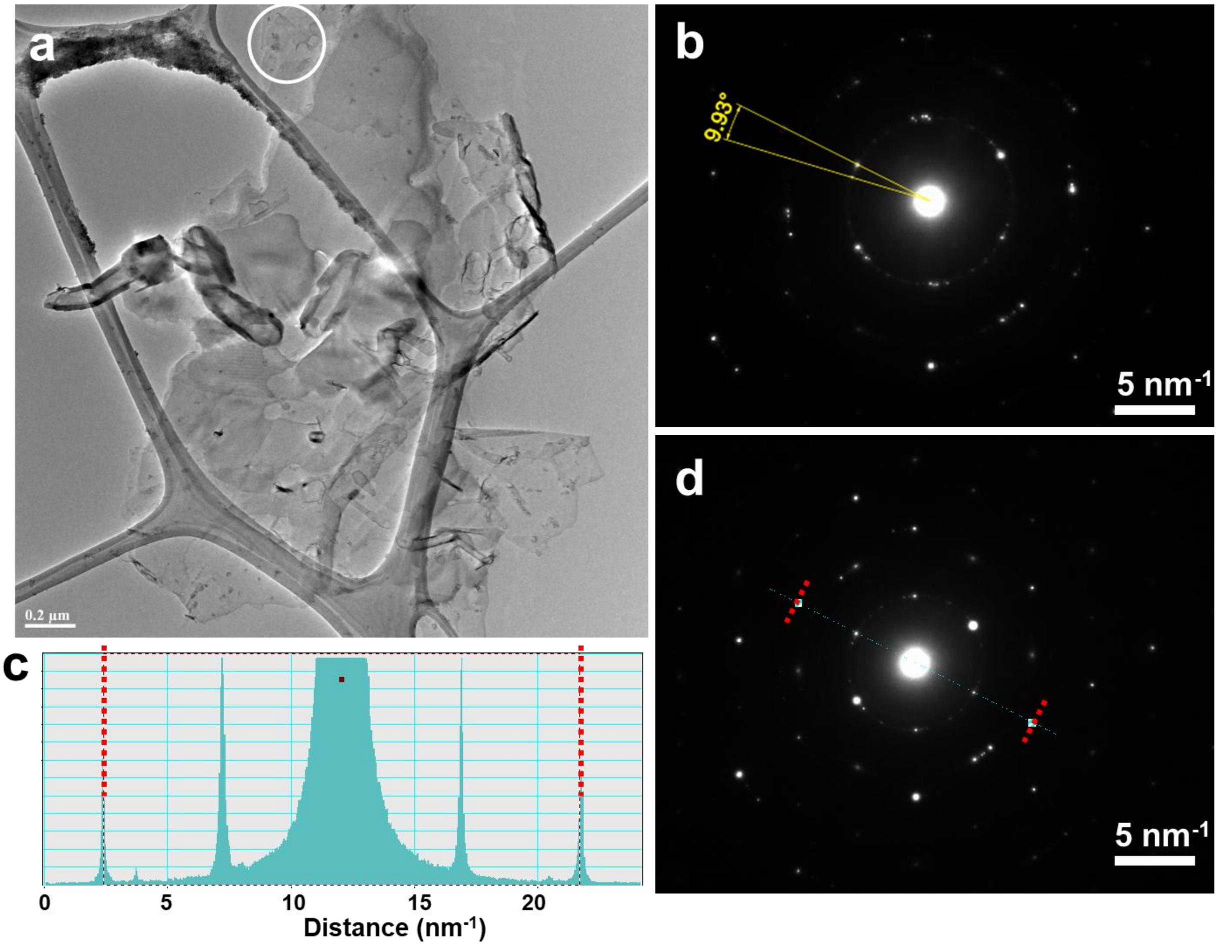

补充图10. 咖啡衍生FG的SAED。 C-FG薄片的TEM图像和
Supplementary Fig. 10. **SAED of coffee-derived FG**. a. TEM image of a C-FG flake and the
SAED的位置。 显示层间错位的几层石墨烯位置的SAED。
position for SAED. b. SAED of the few-layer graphene position that show misalignment
先前研究中与SLG相关的SLG的SAED。
between layers. c-d. SAED of a SLG that correlates with SLG in previous studies.[28, 29]

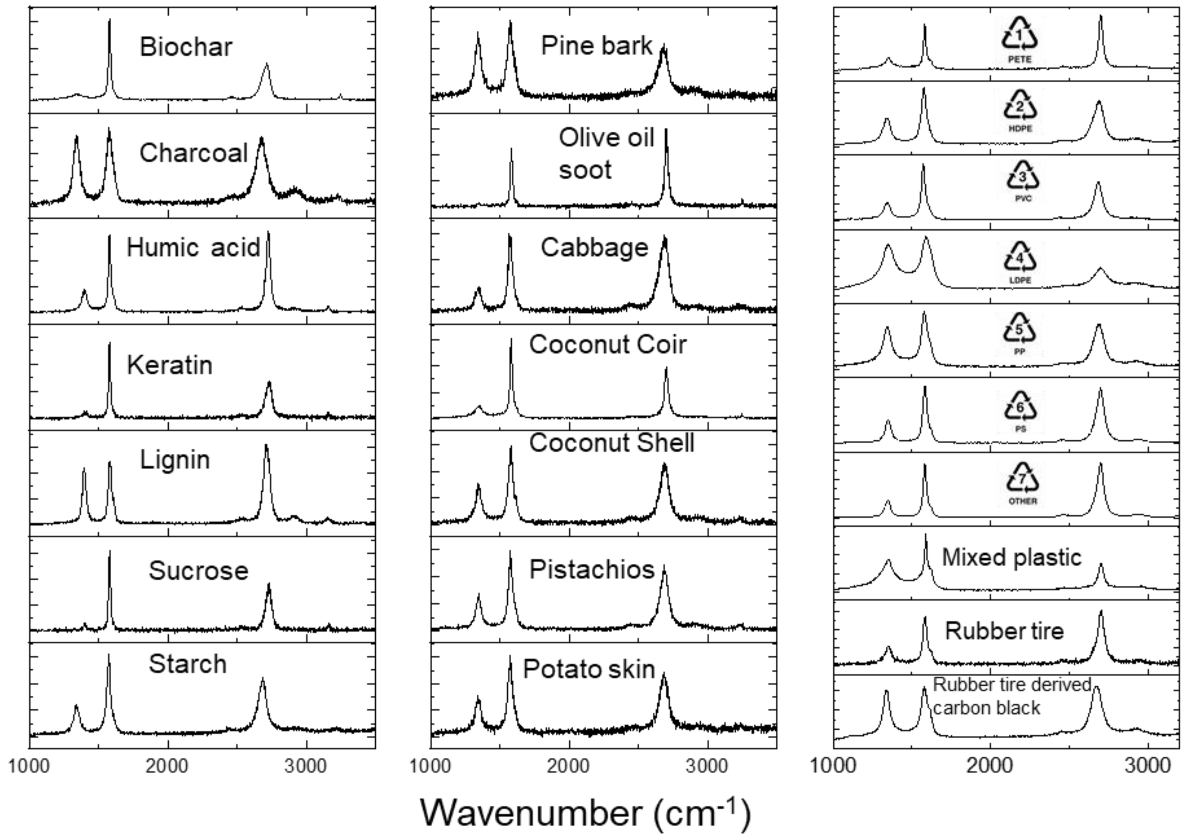

补充图11。来自其他碳源的FG的代表性拉曼光谱。
Supplementary Fig. 11. Representative Raman spectra of FG derived from other carbon sources.
这些都没有针对FJH条件进行优化，以最大限度地提高石墨烯质量。
None of these have been optimized for FJH conditions to maximize the graphene quality.
生物炭具有足够的导电性；它不需要添加剂。所有其他非塑料样品都添加了5至10 wt%的炭黑，以增加其电导率。
Biochar was sufficiently conductive; it needed no additive. All other non-plastic samples had 5 to 10 wt% CB added to increase their conductivities.
所有塑料样品都添加了5 wt%的炭黑以增加其电导率。
All plastic samples had 5 wt% CB added to increase their conductivities.
或者可以使用先前运行的2-5 wt%FG代替炭黑作为导电添加剂，但此处未显示这些光谱。
Or 2 to 5 wt% of FG from a previous run can be used to substitute the CB as the conductive additive, but those spectra are not shown here.
#7其他塑料为聚丙烯腈(PAN)。
#7 plastic, “OTHER”, is polyacrylonitrile (PAN).
混合塑料由以下重量百分比的聚合物制成：HDPE 40%、PETE 40%、PP 10%、PVC 10%。
Mixed plastic was made from the following wt% of polymers: HDPE 40%, PETE 40%, PP 10%, PVC 10%.

补充表4。补充图11的前体源。松树皮、橄榄油烟尘、卷心菜、人发角蛋白、椰子、开心果壳、土豆皮、
Supplementary Table 4. Precursor sources for Supplementary Fig. 11. Pine bark, olive oil soot,
PETE、HDPE、PVC、LDPE、PP和PS作为废物收集，因此未购买。
cabbage, keratin from human hair, coconut, pistachio shells, potato skins, PETE, HDPE, PVC, LDPE, PP, and PS were collected as waste products, so they were not purchased.

生物炭 Biochar	Neroval LLC, from mixed Tennessee 硬木，在1100 ° C下商业化制备 hardwoods, commercially prepared at 1100°C
木炭 Charcoal	Sigma CAS: 7440-44-0
腐殖酸 Humic acid	Sigma CAS: 1415-93-6
木质素 Lignin	Sigma CAS: 8068-05-1
蔗糖 Sucrose	Sigma CAS: 57-50-1
淀粉 Starch	无Argo面筋 Argo gluten free
PAN	Sigma CAS: 25014-41-9
橡胶轮胎衍生炭黑Ergon沥青和乳液股份有限公司。 Rubber tire-derived carbon black	Ergon Asphalt and Emulsion Inc.

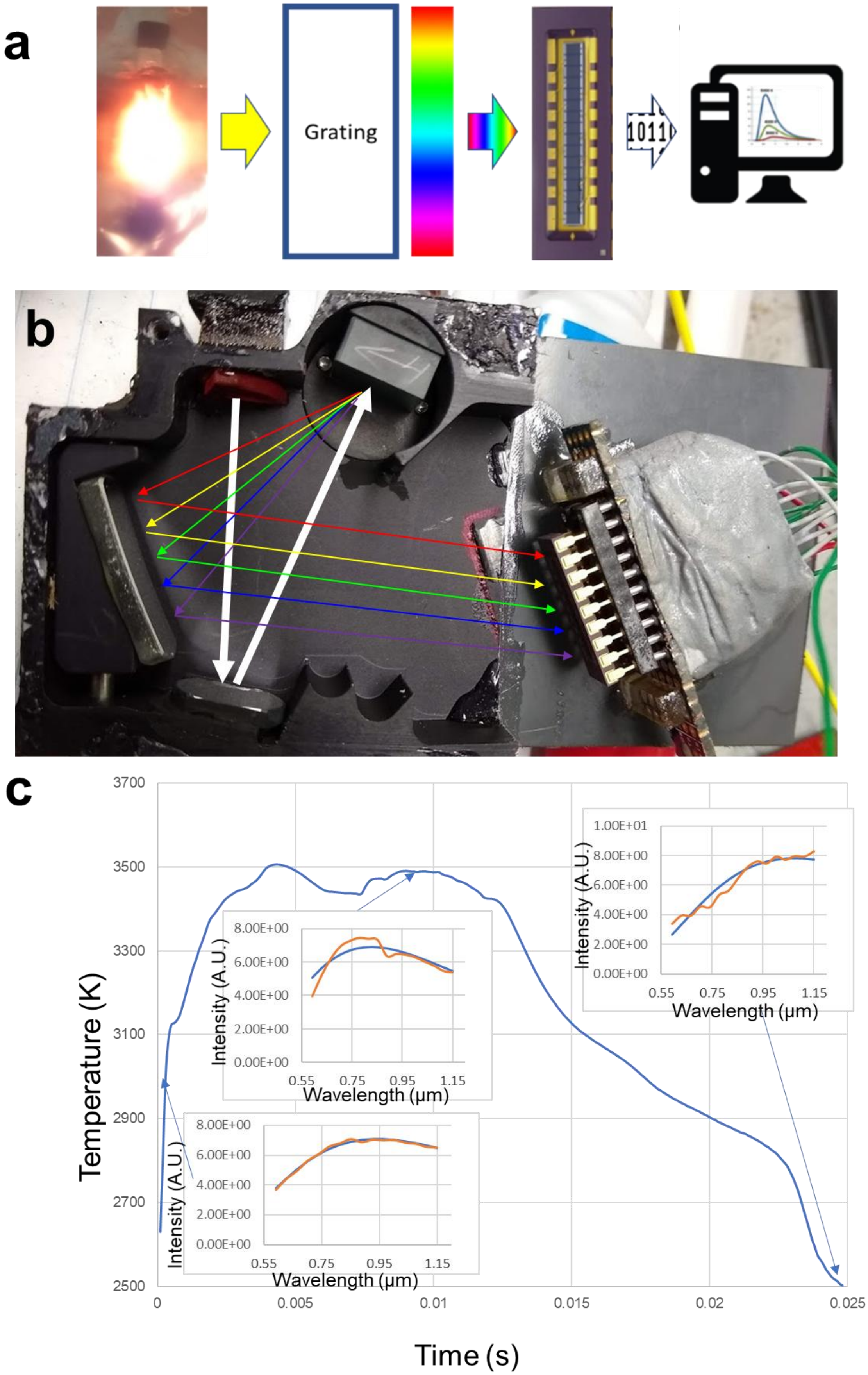

a
Grating
1011
b
c
Temperature (K)
Time (s)
Intensity (A.U.)
Wavelength (μm)

补充图12。超快温度测量。 自制温度测量装置示意图。
Supplementary Fig. 12. Ultrafast temperature measurement. a. Schematic of the home-built

样品的黑体辐射由光纤通过定制的光栅黑匣子收集。
temperature measurement set up. b. Black body radiation from the sample is collected by an

辐射光谱分布在600 nm至1100 nm的16像素光
optical fiber through a customized grating black box. The spectrum of the radiation populates a

电二极管阵列(Hamamatsu S4111-16R)中。 光路如图所示。
16 pixels photodiode arrays (Hamamatsu S4111-16R) at 600 nm to 1100 nm. Light paths are

来自光电二极管阵列的反向偏置电压(9 V)由国家仪器多功能输入/输出设备PCIe-6320
illustrated. The reversed bias voltages (9 V) from the photodiode arrays are collected by the

收集。c 黑体辐射配件。
National Instrument multifunction I/O device PCIe-6320. c. Black body radiation fitting. The

温度-时间曲线图中每个点的温度由0.6-1.1m发射光谱的黑体辐射拟合确定。
temperature from each point of the temperature *vs* time graph is determined by the black body

插图是3000 K、3500 K和2500 K的频
radiation fitting of the spectrum from 0.6-1.1 μm emission. Inset is spectrum fitting for 3000 K,

谱拟合。
3500 K and 2500 K.

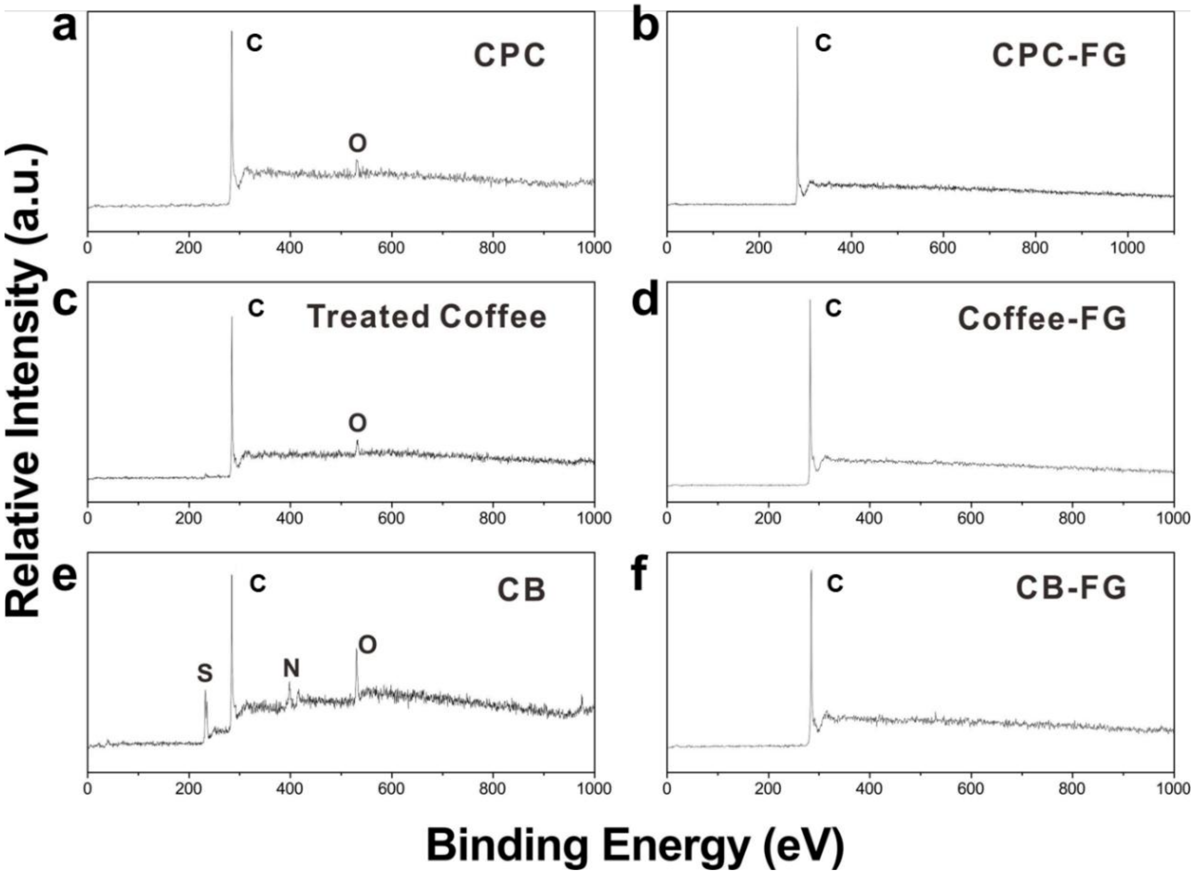

补充图13。FJH工艺前后煅烧石油焦、预处理(见正文)咖啡渣和炭黑的XPS。

Supplementary Fig. 13. XPS of calcined petroleum coke, pre-treated (see main text) coffee grounds and carbon black before and after the FJH process. Significant reduction in contaminants is seen with FG from carbon black.

炭黑的FG可显著减少污染物。

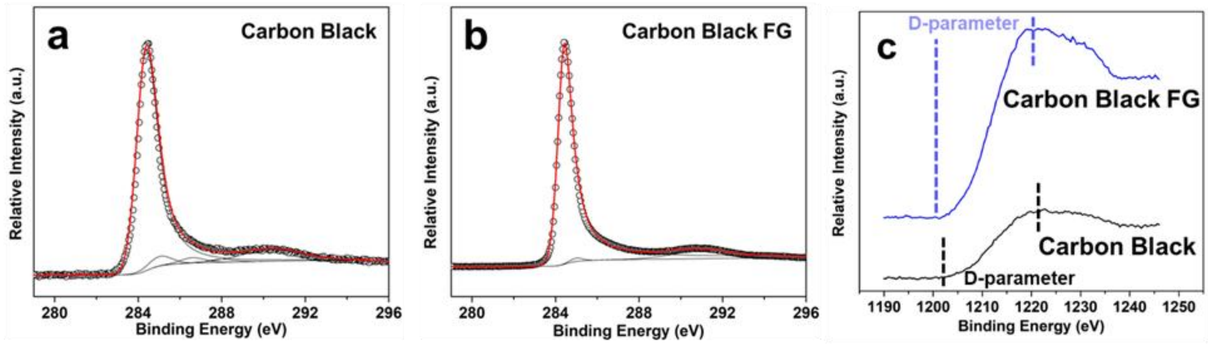

d	C=C (sp2)	C-C (sp3)	C-O/C-O-C	O-C=O/C=O
CB (%)	90.9	4.7	2.8	1.6
CB-FG (%)	98.6	1.4	0	0

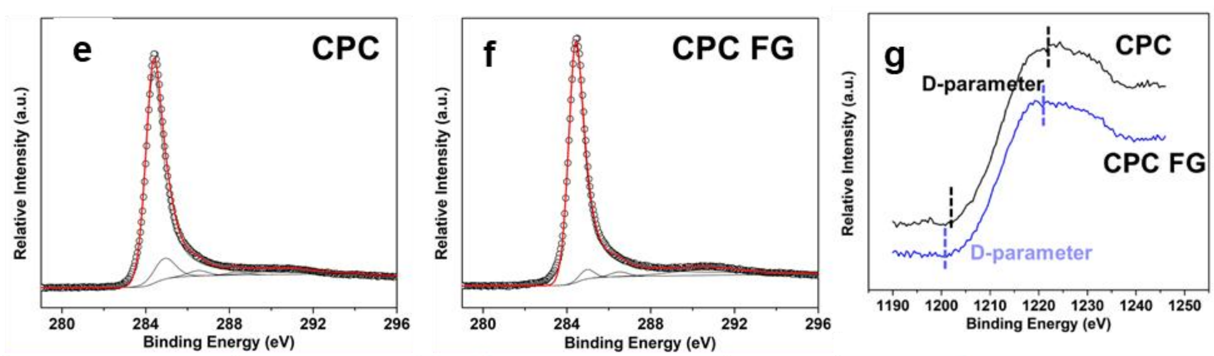

h	C=C (sp2)	C-C (sp3)	C-O/C-O-C	O-C=O/C=O
CPC (%)	84.7	11.1	2.6	1.5
CPC-FG (%)	93.9	3.7	2.4	0

补充图14。CB-FG和CPC碳1s光谱的高分辨率XPS-

Supplementary Fig. 14. **High resolution XPS of the C 1s spectrum from CB-FG and CPC-**

CB和CB-FG的C KLL光谱的高分辨率XPS。

FG. a. CB. b. CB-FG. c. High resolution XPS of C KLL spectrum of CB and CB-FG. The D-

D参数衡量微分C KLL谱中最大值和最小值之间的能量分离。

parameter measures the energy separation between maxima and minima in differentiated C KLL

在金刚石和石墨烯中，其值分别为13 eV和21 eV。 值越大，则

spectra. In diamond and graphene, the values are 13 eV and 21 eV, respectively. The larger

表明sp2/sp3比率越高。 对于CB和CB-FG，值分别为20.5 eV和20.9 eV。

values infer a higher sp^2/sp^3 ratio.[30] For the CB and CB-FG, the values are 20.5 eV and 20.9 eV,

因此，在FJH过程之后，sp2/sp3比率在从CB到CB-FG的过程中增加。

respectively. Thus, after the FJH process, the sp^2/sp^3 ratio increases in going from CB to CB-FG.

CB和CB-FG的反卷积C 1s峰值高分辨率谱的相对分布。
d. Relative distribution of deconvoluted C 1s peak high resolution spectrum of CB and CB-FG.
sp2碳(C=C)的相对分布从90.9%增加到98.6%，sp3碳(C-
Relative distribution of sp^2-carbon (C=C) increases from 90.9% to 98.6% and the sp^3-carbon (C-
C) 从4.7%降至1.4%。 因此，FJH过程后，sp2/sp3比率增加，与CB-FG的拉曼光谱中
C) decreases from 4.7 % to 1.4 %. Thus, the sp^2/sp^3 ratio increases after the FJH process,
非常高的2D/G比率有关。
corroborating with the very high 2D/G ratio in the Raman spectra of CB-FG. d. Relative
CPC和CPC-FG的反卷积C 1s峰值高分辨率谱的相对分布。
distribution of deconvoluted C 1s peak high resolution spectrum of CPC and CPC-FG. The
FJH工艺后，sp2/sp3比率从7.6增加到25.2，证实了
sp^2/sp^3 ratio increases from 7.6 to 25.2 after the FJH process, corroborating with the very high
CPC-FG拉曼光谱中的2D/G比。
2D/G ratio in the Raman spectra of the CPC-FG.

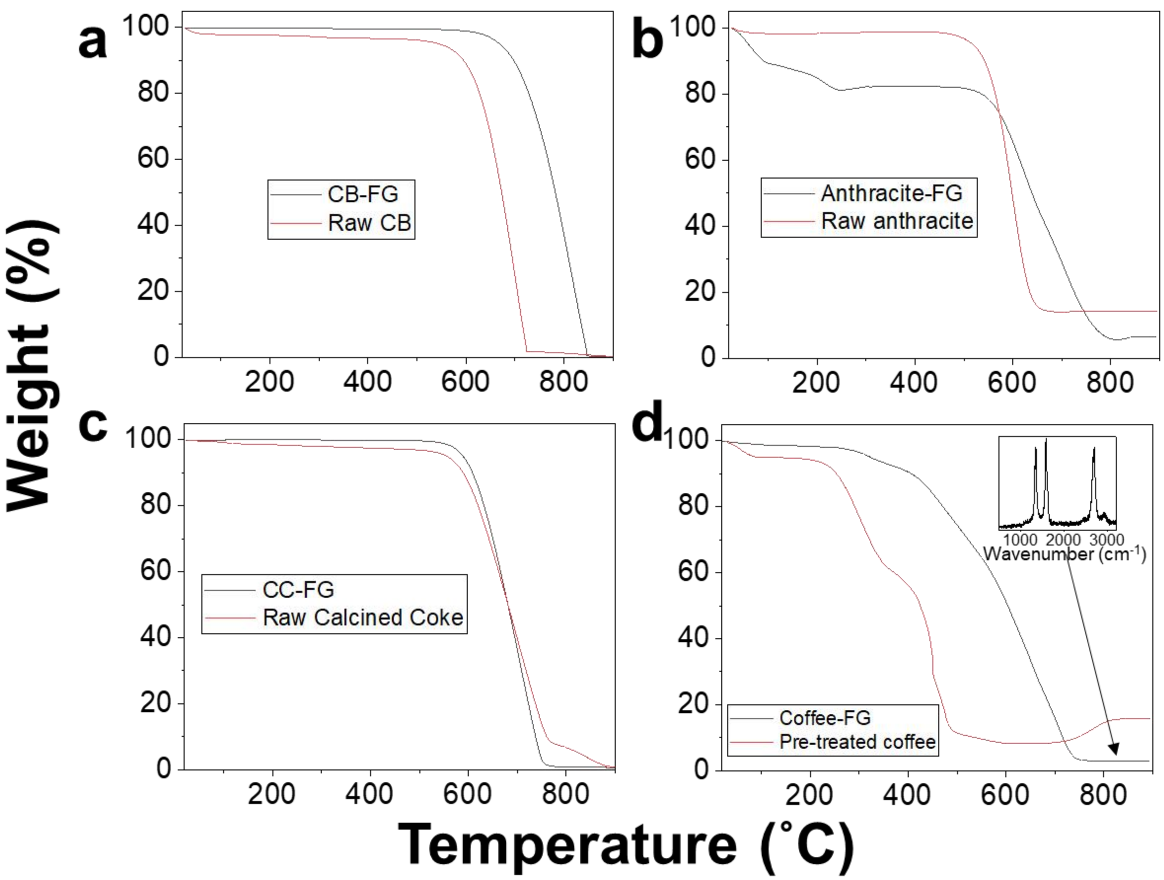

补充图15。空气中TGA：a. 生CB(黑珍珠2000，卡博特)和CB-FG。
Supplementary Fig. 15. TGA in air of: a. Raw CB (Black Pearls 2000, Cabot) and CB-FG. b.
原煤无烟煤和无烟煤FG。 生煅烧焦炭和CC-FG。 预处理咖啡
Raw anthracite coal and anthracite-FG. c. Raw calcined coke and CC-FG. d. Pre-treated coffee

和咖啡FG。 对于炭黑、无烟煤和咖啡，前体材料和衍生FG之间的最终重量显著减少。
and coffee-FG. With carbon black, anthracite coal and coffee, there is significant decrease in the
TGA残渣的XPS分析表明，无烟煤FG
final weight between the precursor material and the derived FG. XPS of the TGA residue shows
的TGA残渣中含有C(15%)、O 62%、Si(11%)和Al(12.6%)；咖啡FG残渣中含有C(65%)、O(25%
that the TGA-residue from anthracite-FG contains of C (15%), O 62 %, Si (11%) and Al (12.6%);
)、S(2.9%)和P(2%)。 此外，通过拉
and residue from coffee-FG contains of C (65%), O (25%), S (2.9%) and P (2%). Furthermore,
曼光谱(插图d)对咖啡FG中的TGA残留物进行了分析，表明其明显是石墨烯。
the TGA-residue from coffee-FG was analyzed by Raman spectroscopy (inset in d) to show that
it is significantly graphene.

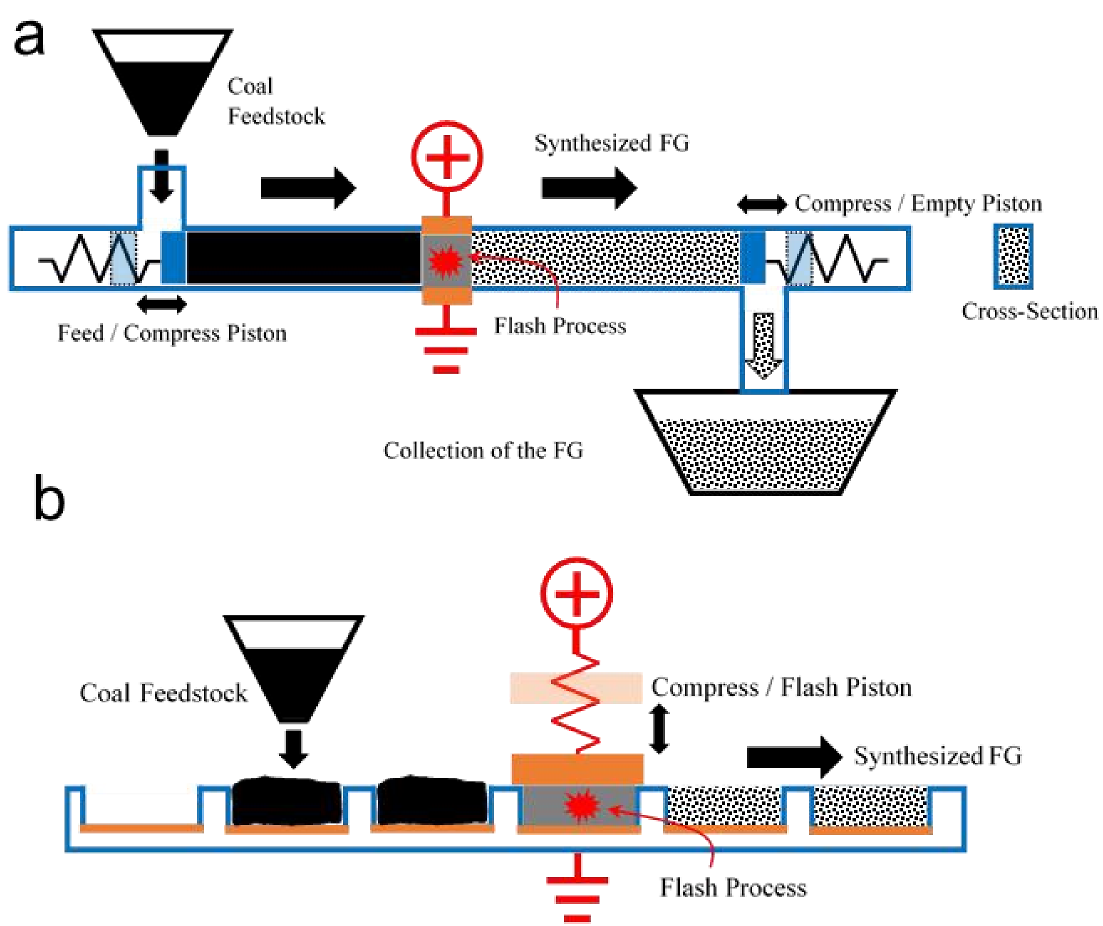

补充图16。FG过程自动化的可能反应器，例如煤源。
Supplementary Fig. 16. Possible reactors for automation of the FG process, for example with a
连续活塞FG工艺。 与实验室设置不同，压缩活塞和电极的功能由单独的
coal source. a. Continuous piston FG process. Unlike the laboratory setup, the function of the
部件执行。 合适的电
compression pistons and the electrodes is carried out by separate components. Suitable
极为铜、不锈钢、石墨或钨电极，这些电极连接在石英上，但有通风孔，以便在FJH工艺过程中排出热工
electrodes are copper, stainless steel, graphite or tungsten electrodes that are attached to the
艺气体。
quartz but have vent holes to enable escape of the hot process gases during the FJH process. The
压缩活塞可以由介电材料制成，可能是石英或陶瓷，以防止对活塞接地短路。
compression pistons can be made of a dielectric material, possibly quartz or ceramic, to prevent
在这一连续过程中，碳原料通过储罐进入过程管(由振动筛辅助)，
shorting to the piston's ground. In this continuous process, carbon feedstock is fed through a
同时压缩活塞向左缩回。
reservoir into the process tube (aided by a shaker) while the compression piston is retracted to
在管中分配碳粉后，进料压缩活塞以足够的行程移动，以从电极下方(JH区域)置换转化的碳，
the left. After the carbon powder is dispensed in the tube, the Feed Compress Piston moves with
同时空的压缩活塞向右收缩，以允许FG排空到收集箱中(借助于振动筛或真空吸力)。
enough stroke to displace the converted carbon from underneath the electrodes (JH region) while
at the same time the Empty Compress Piston retracts to the right to allow FG to be emptied into a
冲击结束后，空活塞推入以堵塞管道，同时给
collection bin (aided by a shaker or a vacuum suction). After the strike is over, the Empty Piston
煤活塞向煤施加预定压力，直到FJH过程完成。
pushes in to block the tube while the Feed Piston applies predetermined pressure to the coal until
活塞循环需要与连续过程的吞吐量相匹配。
the FJH process is done. The piston cycles need to match the throughput of the continuous
碳/FG材料的流动是在一个封闭的环境中进行的，这使得操作安全。
process. The flow of carbon/FG material is in an enclosed environment that makes the operation
连续皮带FG工艺。 在该反应中，煤原料通过蓄水池进入石英或陶瓷舟，该舟具有金属底
safe. b. Continuous Belt FG Process. In this reaction, the coal feedstock is fed through a reservoir
部电极，该电极接地，是连续皮带的一部分。
into the quartz or ceramic boat, having a metallic bottom electrode that is grounded electrically,
and is part of a continuous belt.

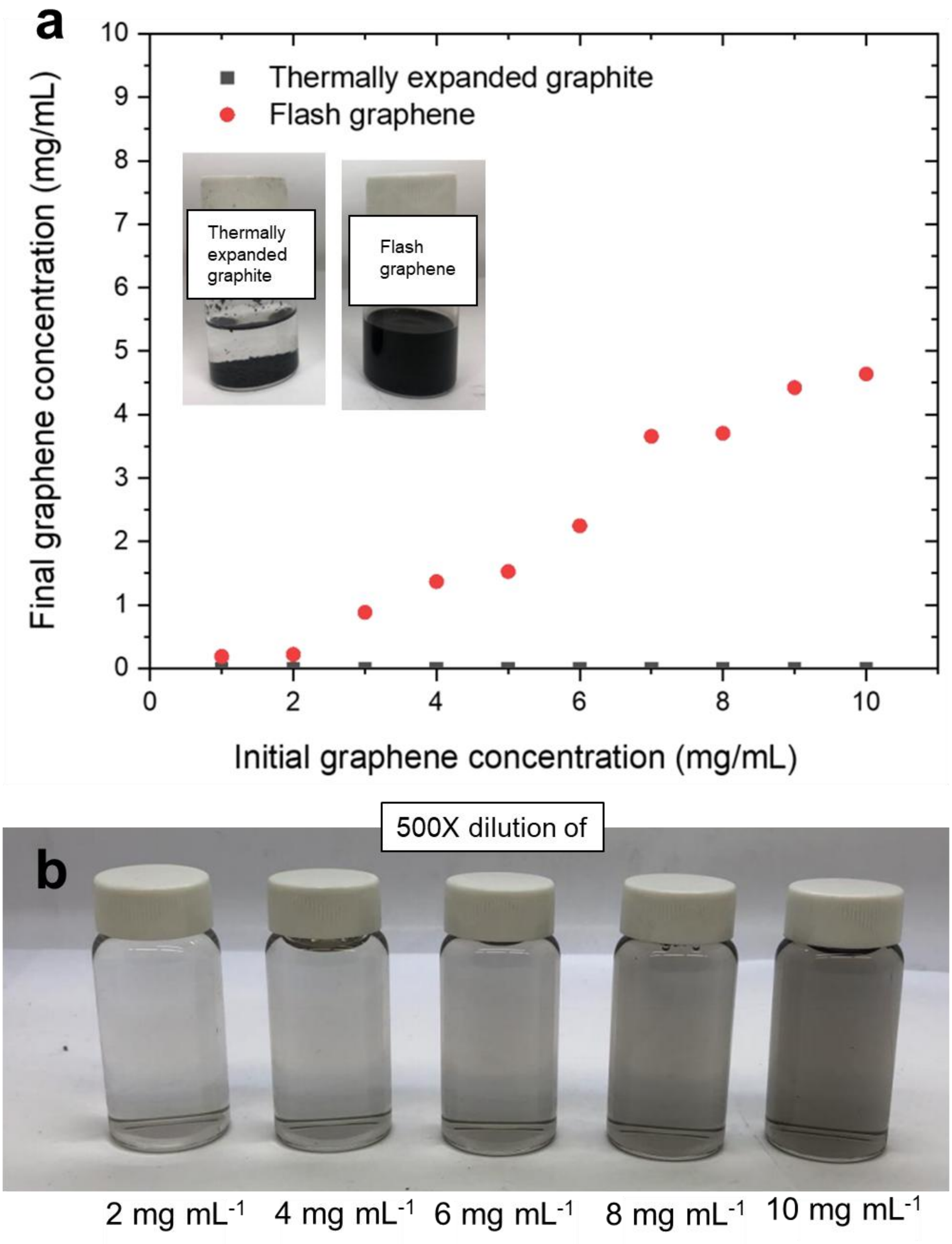
a
Final graphene concentration (mg/mL)
Initial graphene concentration (mg/mL)
Thermally expanded graphite
Flash graphene
Thermally expanded graphite
Flash graphene
0
1
2
3
4
5
6
7
8
9
10
0
2
4
6
8
10
500X dilution of
b
2 mg mL-1
4 mg mL-1
6 mg mL-1
8 mg mL-1
10 mg mL-1

补充图17. FG在水/Pluronic(F-127)(1%)中的分散性。
Supplementary Fig. 17. FG dispersion in water/Pluronic (F-127) (1%). a. Comparison of
5 mg mL-1热膨胀石墨和CB-FG在水/Pluronic(F-127)(1%)中的分散性比较。
dispersibility of 5 mg mL^{-1} of thermally expanded graphite and CB-FG in water/Pluronic (F-127)
热膨胀石墨在离心后沉降(见方法)，而CB-FG仍分散在水表面活性剂溶液中。
(1%). The thermally expanded graphite settles after centrifugation (see Methods) while the CB-
CB-FG的视觉分散性。
FG remains dispersed in the water surfactant solution. b. Visual dispersibility of CB-FG. The
原始浓度在图像下方指定，但该浓度稀释了500倍，以直观显示CB-FG的分散性。
original concentration is specified below the image but that concentration was diluted 500x for
所有稀释溶液中均未发现大颗粒。
visual demonstration of CB-FG dispersibility. No large particles are found visually in all diluted solutions.

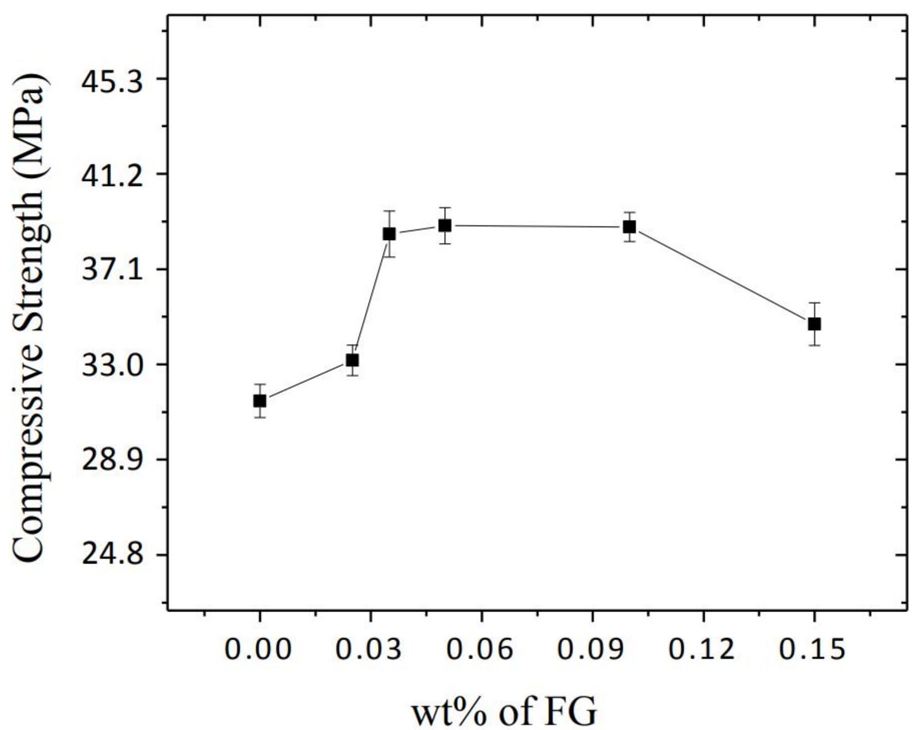

补充图18。CB-FG/水泥复合材料的力学性能
Supplementary Fig. 18. Mechanical properties of the CB-FG/cement composites measured at
28天。
28 days.

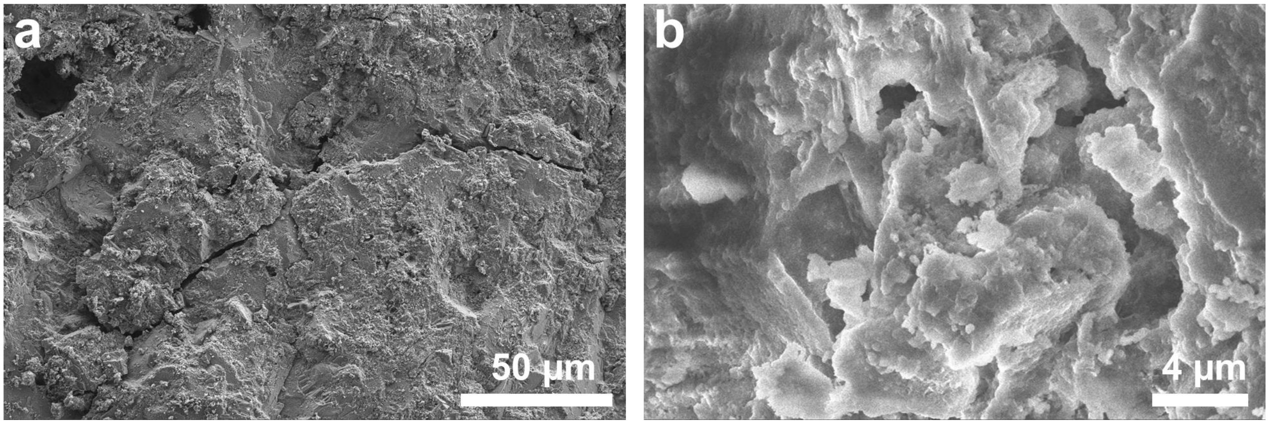

补充图19。 水泥和CB-FG复合材料的SEM图像。 SEM图像显示石墨烯在硅酸
Supplementary Fig. 19. SEM images of cement and CB-FG composite. The SEM images show
盐水泥中分散良好，没有任何可见的大石墨烯片。
good graphene dispersion in Portland cement without any visible large flakes of graphene.

CB-FG/水泥复合材料性能的大幅提高可能是由于涡轮层流CB-FG在水中易于分散，均匀分布的片状FG作为模板
The large enhancement in the properties of CB-FG/cement composites could be due to the ease
，促进水泥水合物产品的一致生长。
of dispersibility of the turbostratic CB-FG in water where the homogenously distributed sheet-like FG acts as templates to promote congruent growth of cement hydrate products.[31]
此外，有文献表明，石墨烯和水泥水合物产品之间的共价C-O键/网络可以在共价键形成时改变石墨烯从sp2
Additionally, there is literature suggestion that covalent C-O bonds/networks between graphene
到sp3的杂化，大大提高复合材料的机械性能，尽管我们无法验证或证实该反应的机理。
and cement hydrate products can change the hybridization of graphene from sp^2 to sp^3 upon covalent bond formation, greatly enhancing the mechanical properties of the composite, though
有人认为，这种变化以及界面区域
we cannot verify or substantiate the mechanism for that reaction.[32] It has been suggested that this
附近的电子释放，可导致性能改善的均质、互混和插层复合材料。
change, along with electron release in the vicinity of their interfacial region, can lead to
这是否发生在这
homogenous, inter-mixed and intercalated composites with improved properties. Whether this is
里还没有得到实验验证。
taking place here has not been experimentally verified.

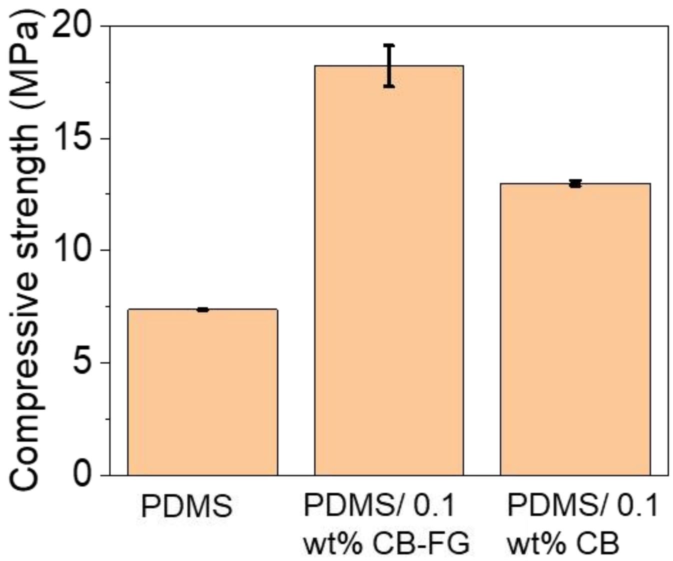

补充图20。PDMS、CB-FG/PDMS复合材料和
Supplementary Fig. 20. Compressive strength of PDMS, CB-FG/PDMS composite and
CB/PDMS复合材料。
CB/PDMS composite.

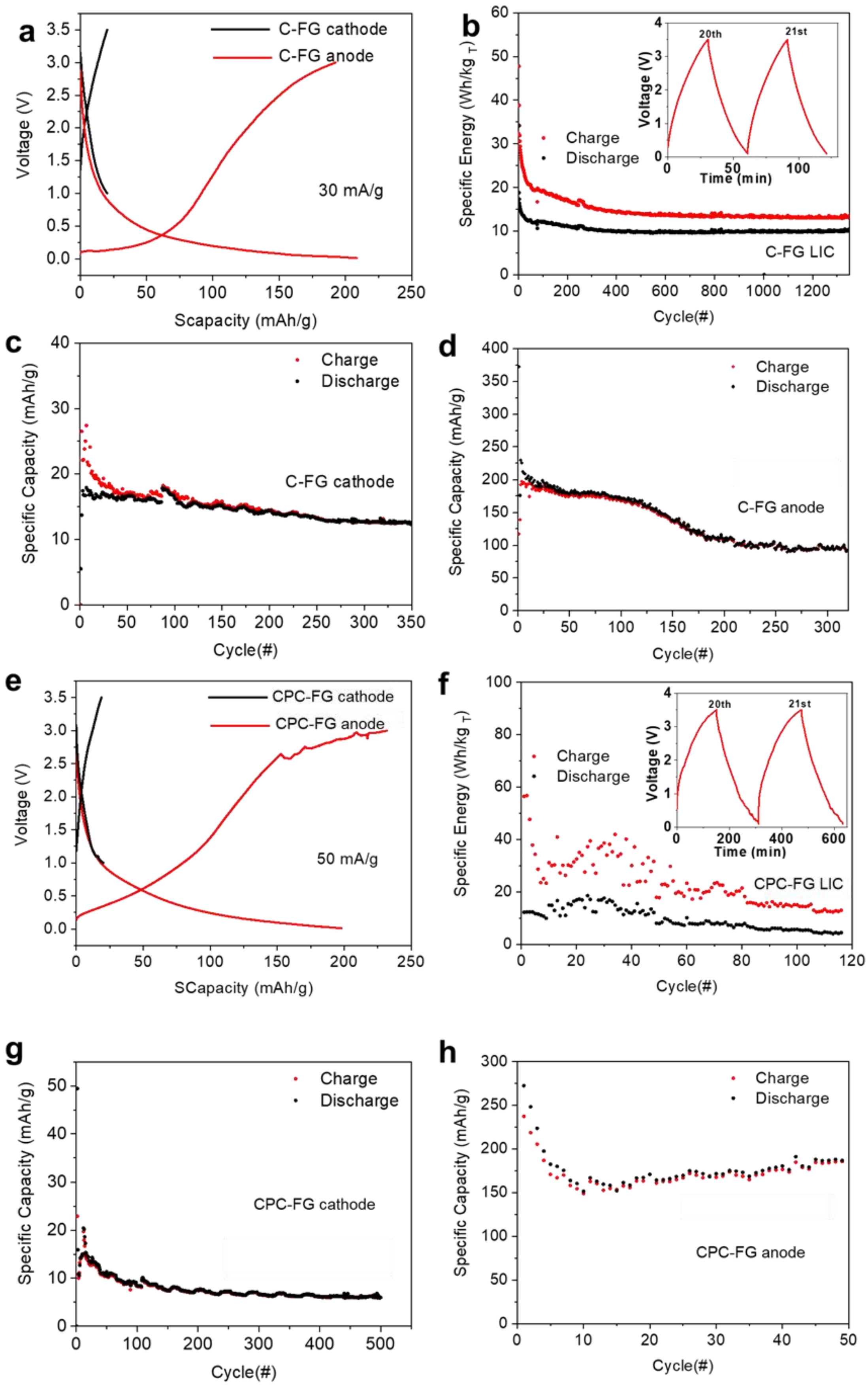
a
C-FG cathode
C-FG anode
30 mA/g
Voltage (V)
Scapacity (mAh/g)
b
Specific Energy (Wh/kg T)
Charge
Discharge
20th
21st
Voltage (V)
Time (min)
C-FG LIC
Cycle(#)
c
Charge
Discharge
C-FG cathode
Specific Capacity (mAh/g)
Cycle(#)
d
Charge
Discharge
C-FG anode
Specific Capacity (mAh/g)
Cycle(#)
e
CPC-FG cathode
CPC-FG anode
50 mA/g
Voltage (V)
SCapacity (mAh/g)
f
Specific Energy (Wh/kg T)
Charge
Discharge
20th
21st
Voltage (V)
Time (min)
CPC-FG LIC
Cycle(#)
g
Charge
Discharge
CPC-FG cathode
Specific Capacity (mAh/g)
Cycle(#)
h
Charge
Discharge
CPC-FG anode
Specific Capacity (mAh/g)
Cycle(#)

补充图21。FG在锂离子电容器和锂离子电池中。 制作锂离子电池并循环，
Supplementary Fig. 21. FG in a Li-ion capacitor and a Li-ion battery. A Li-ion battery was
然后打开电池，使用阳极和阴极制作锂离子电容器。
made and cycled, then the battery was opened and the anode and cathode were used to make the
在以锂箔作为计数器和参比电极的半电池中，具有C-FG阳极(0.01 3.0 V)和阴极(
Li-ion capacitor. a. Charge/discharge curves of the Li-ion battery with C-FG anodes (0.01−3.0 V)
1 3.5 V)的锂离子电池的充放电曲线。
and cathodes (1−3.5 V) in half-cells with Li foil as the counter and reference electrode. b. Long-
C-FG锂离子电容器在20 mA时的长期稳定性。g-1。c 采用C-FG阴极半电池的锂离子电池在30
range stability of C-FG Li-ion capacitor at 20 $mA.g^{-1}$. c. Cycling performance of the Li-ion
mA时的循环性能。g-1。d 以C-FG为阳极半电池的锂离子电池在50
battery with the C-FG cathode half-cell at 30 $mA.g^{-1}$. d. Cycling performance of the Li-ion
mA时的循环性能。e. 采用煅烧石油焦FG(CPC-FG)阳极(0.01 3.0 V)和阴极(1 3.5
battery with C-FG as the anode half-cell at 50 $mA.g^{-1}$. e. Charge/discharge curves of the Li-ion
V)的锂离子电池在以锂箔作为对电极和参比电极的半电池中的充放电曲线。
battery with calcined petroleum coke-FG (CPC-FG) anode (0.01−3.0 V) and cathode (1−3.5 V)
CPC-FG锂离子电容器在5 mA
in half-cells with Li foil as the counter and reference electrode. f. Long-range stability of the
时的长期稳定性g. 以CPC-FG为阴极的锂离子电池在25 mA时的循环性能。g-1。h。
CPC-FG Li-ion capacitor at 5 $mA.g^{-1}$. g. Cycling performance of the Li-ion battery with CPC-
以CPC-FG为阳极半电池的锂离子电池在100 mA时的循环性能。g-1。
FG as cathode at 25 $mA.g^{-1}$. h. Cycling performance of the Li-ion battery with CPC-FG as the
anode half-cell at 100 $mA.g^{-1}$.

电化学测试方法
Electrochemical Test Protocols

在CR2032电池上测试了闪蒸石墨烯的电化学性能。 所有细胞在氩
The electrochemical performance of flashed graphene was tested in CR2032 cells. All the cells
气气氛下组装在手套箱中。 CR2032锂离子电池由锂箔作为对电极，
were assembled in a glove box under argon atmosphere. The CR2032 lithium-ion cell consists of
Celgard K2045作为分离器，1 M六氟磷酸锂(LiPF6)溶解在1:1:1的碳酸乙烯酯：碳酸
lithium foil as the counter electrode, Celgard K2045 as the separator, 1 M lithium
二甲酯：碳酸二乙酯(EC:DMC:DEC)(MTI corporation
hexafluorphosphate (LiPF6) dissolved in 1:1:1 ethylene
)中作为电解液，FG(C-FG和CC-FG)作为阴极/阳极组成。
carbonate:dimethylcarbonate:diethylcarbonate (EC:DMC:DEC) (MTI corporation) as the
阴极/阳极是通过将含有80%(重量百分
electrolyte, and FG (C-FG and CC-FG) as cathode/anode. The cathode/anode were prepared by
比)活性材料、10%(Super P，TIMCAL)和10%(重量百分比)聚偏二氟乙烯(PVDF；Alfa Aesar)
casting slurry which consists 80 wt% active material, 10 wt% (Super P, TIMCAL) and 10 wt%
的浆料在N-甲基-2-吡咯烷酮(NMP)中涂布在一片铝/铜箔上制备的。
polyvinylidene difluoride (PVDF; Alfa Aesar) in *N*-methyl-2-pyrrolidone (NMP) on a piece of
恒流放电/充电试验在0.01至
Al/Cu foil. The galvanostatic discharge/charge tests were carried out in voltage range of 0.01 to

阳极为3.0 V(vs Li+/Li)，阴极为1.0至3.5 V(vs Li+/Li)。
3.0 V (vs Li+/Li) for anode and 1.0 to 3.5 V (vs Li+/Li) for cathode, respectively. The full
在CR2032电池上测试了锂离子电容器中闪蒸石墨烯的全电容性能。
capacitor performance of flashed graphene in the Li-ion capacitor was tested in CR2032 cells. In
为了组装FG锂离子电容器，锂离子电池半电池的阳极和阴极循环数次，阳极处于放电状态，阴极处于充电状态。
order to assemble the FG Li-ion capacitor, the anode and cathode of the Li-ion battery half-cells were cycled several times with the anode rested at the discharge state and cathode rested at the charge state.
在手套箱内打开两个电池，重新组装成FG锂离子电容器，并在0.1至3.5V的电压范围内进行测试。
The two cells were opened inside a glovebox, re-assembled as a FG Li-ion capacitor, and tested in the voltage range of 0.1 to 3.5 V.
锂离子电容器的容量是根据锂离子电池阳极和阴极的总质量计算的。
The capacity of Li-ion capacitor was calculated based on the total mass of the anode plus cathode that had come from the Li-ion battery.

References

1 Novoselov, K. S. *et al.* Electric field effect in atomically thin carbon films. *Science* **306**, 666-669 (2004).

2 Allen, M. J. *et al.* Honeycomb carbon: a review of graphene. *Chem. Rev.* **110**, 132-145 (2009).

3 Partoens, B. & Peeters, F. M. From graphene to graphite: Electronic structure around the K point. *Phys. Rev. B* **74**, 075404 (2006).

4 Malard, L. M. *et al.* Raman spectroscopy in graphene. *Phys. Rep.* **473**, 51-87 (2009).

5 Bianco, A. *et al.* All in the graphene family – A recommended nomenclature for two-dimensional carbon materials. *Carbon* **65**, 1-6 (2013).

6 Yan, Z. *et al.* Hexagonal graphene onion rings. *J. Am. Chem. Soc.* **135**, 10755-10762 (2013).

7 Kim, K. *et al.* Raman spectroscopy study of rotated double-layer graphene: misorientation-angle dependence of electronic structure. *Phys. Rev. Lett.* **108**, 246103 (2012).

8 Kato, H. *et al.* Growth and Raman spectroscopy of thickness-controlled rotationally faulted multilayer graphene. *Carbon* **141**, 76-82 (2019).

9 Niilisk, A. *et al.* Raman characterization of stacking in multi-layer graphene grown on Ni. *Carbon* **98**, 658-665 (2016).

10 Kiselov, V. *et al.* The growth of weakly coupled graphene sheets from silicon carbide powder. *Semicond. Phys., Quantum Electron. Optoelectron.* 301-307 (2014).

11 Garlow, J. A. *et al.* Large-area growth of turbostratic graphene on Ni (111) via physical vapor deposition. *Sci. Rep.* **6**, 19804 (2016).

12 Ferrari, A. C. *et al.* Raman spectrum of graphene and graphene layers. *Phys. Rev. Lett.* **97**, 187401 (2006).

13 Novoselov, K. S. *et al.*Two-dimensional gas of massless Dirac fermions in graphene. *Nature* **438**, 197 (2005).

14 Ferrari, A. C. Raman spectroscopy of graphene and graphite: Disorder, electron–phonon coupling, doping and nonadiabatic effects. *Solid State Commun.* **143**, 47-57 (2007).

15 Kudin, K. N. *et al.* Raman spectra of graphite oxide and functionalized graphene sheets. *Nano Lett.* **8**, 36-41 (2008).

16 Ni, Z. H. *et al.* Probing Charged Impurities in Suspended Graphene Using Raman Spectroscopy. *ACS Nano* **3**, 569-574 (2009).

17 Ferrari, A. C. & Basko, D. M. Raman spectroscopy as a versatile tool for studying the properties of graphene. *Nat. Nano.* **8**, 235 (2013).

18 Kumar, N. *et al.* High-temperature phase transformation and low friction behaviour in highly disordered turbostratic graphite. *J. Phys. D: Appl. Phys.* **46**, 395305 (2013).

19. Yan, Zheng *et al.* Toward the Synthesis of Wafer-Scale Single-Crystal Graphene on Copper Foils. *ACS Nano* **6**, 9110-9117 (2012).

20. Franklin, R. E. Crystallite growth in graphitizing and non-graphitizing carbons. *Proc. R. Soc. Lond. A.* **209**, 196-218 (1951).

21. Harris, P. J. F. & Tsang, S. C. High-resolution electron microscopy studies of non-graphitizing carbons. *Philos. Mag. A* **76**, 667-677 (1997).

22. Iijima, S. Direct observation of the tetrahedral bonding in graphitized carbon black by high resolution electron microscopy. *J. Cryst. Growth* **50**, 675-683 (1980).

23. Huang, J. Y. *et al.* Real-time observation of tubule formation from amorphous carbon nanowires under high-bias Joule heating. *Nano Lett.* **6**, 1699-1705 (2006).

24. Wang, B. *et al.* Electro-graphitization and exfoliation of graphene on carbon nanofibers. *Carbon* **117**, 201-207 (2017).

25. Vander Wal, R. L. *et al.* Carbon nanostructure examined by lattice fringe analysis of high-resolution transmission electron microscopy images. *Appl. Spectrosc.* **58**, 230-237 (2004).

26. Kim, D.-Y., Nishiyama, Y., Wada, M. & Kuga, S. Graphitization of highly crystalline cellulose. *Carbon* **39**, 1051-1056 (2001).

27. Haensel, T. *et al.* Pyrolysis of cellulose and lignin. *Appl. Surf. Sci.* **255**, 8183-8189 (2009).

28. Luo, B. *et al.* Chemical vapor deposition of bilayer graphene with layer-resolved growth through dynamic pressure control. *J. Mater. Chem. C* **4**, 7464-7471 (2016).

29. Li, J. *et al.* Controllable atmospheric pressure growth of mono-layer, bi-layer and tri-layer graphene. *Chem. Commun.* **50**, 11012-11015 (2014).

30. Jalilov, A. S. *et al.* Mechanistic study of the conversion of superoxide to oxygen and hydrogen peroxide in carbon nanoparticles. *ACS Appl. Mater. Interfaces* **8**, 15086-15092 (2016).

31. Moghaddam, S. E. *et al.* Morphogenesis of cement hydrate. *J. Mater. Chem. A* **5**, 3798-3811 (2017).

32. Hosseini, E., Zakertabrizi, M., Korayem, A. H. & Shahsavari, R. Tunable, multifunctional ceramic composites via intercalation of fused graphene boron nitride nanosheets. *ACS Appl. Mater. Interfaces* **11**, 8635-8644 (2019).